Title: Inflammatory Synovial Fibroblast Culture in 3D Systems: A Comparative Transcriptomic and Functional Study.

Aneesah Khan[2], Oana Dobre[1], Yilin Wang[2], Thanutchaporn Sartyoungkul[2], Manuel Salmeron-Sanchez[1], Margaret H. Harnett[2], Miguel A. Pineda[1,3]

[1] Centre for the Cellular Microenvironment, University of Glasgow, 11 Chapel Lane, G11 6EW, Glasgow, UK.

[2] Institute of Infection and Immunity, University of Glasgow, 120 University Place, G128TA, Glasgow, UK.

[3] Corresponding author, miguel.pineda@glasgow.ac.uk

Keywords: 3D culture, inflammation, hydrogels, arthritis, synovial fibroblast.

Abstract

Inflammation is essential for responding to infections and subsequent tissue healing. However, chronic unresolved inflammation can become a serious health problem, as exemplified in the joints during Rheumatoid Arthritis (RA). Why does inflammation persist in RA? The answer could lie with synovial fibroblasts, non-haemopoietic cells that can adopt a pathogenic phenotype that fuels disease progression for years. Critically, targeting local fibroblasts could stop joint inflammation without suppressing systemic immunity. Nevertheless, basic research findings have not been translated to new drugs, perhaps because non-physiological data can be inadvertently generated in 2D cultures. Thus, developing better in vitro platforms is an urgent need in biomedical research. In this work, we sought to understand how distinct 3D environments affect fibroblast-mediated inflammation. Arthritic synovial fibroblasts were expanded and cultured in 2D, 3D rigid scaffolds and engineered hydrogels. The results reveal that SFs are plastic and adopt inflammatory or remission-like phenotypes in response to their surroundings. This work identifies new directions to develop better models for drug testing, and even signposts candidate mechanisms by which to rewire destructive SFs.

Introduction

Stromal cells, such as fibroblasts, were initially described simply as tissue supportive cells whose main function was to produce the matrix in which other cells were embedded. This was particularly true for early immunologists, captivated by the protective and pathogenic roles of the most recognizable immune effector cells. Today we see a different landscape, where fibroblasts are moving to the centre stage in immunology because in addition to their well-established role of providing physical support, fibroblasts define the nature and magnitude of local immune responses. A clear example is the synovial fibroblast (SF), a specialized population found only in the synovium, the tissue lining the inside of the capsule wrapping articular joints such as the shoulder, wrist, knee or ankle. SFs provide nutritional support and synthesise lubricating molecules like hyaluronic acid and lubricin, but they can also secrete inflammatory mediators and control bone remodelling. When this process is dysregulated, SFs can become active disease drivers, as in the joints of Rheumatoid Arthritis (RA) patients. During RA, SFs become hyperproliferative, increase production of matrix-degrading enzymes and promote recruitment and survival of immune system cells(1-4) In turn, immune system cells secrete more inflammatory cytokines, such as IL-6, IL-17 or TNF, consolidating SF-mediated production of inflammatory factors. This results in further recruitment of immune cells and generation of self-sustained inflammatory and bone-destruction loops, a hallmark of chronic inflammation in RA.

Modulation of SFs responses would offer a clinical benefit to RA patients, as it would directly target the core disease tissue to neutralize local autoimmune networks whilst avoiding the adverse effects of current immunosuppressive drugs. However, despite intensive research in the field no drug has been approved to target SFs yet. This might reflect that our understanding of SF-dependent inflammation is based not only on clinical or in vivo studies, but also on cells expanded in vitro on non-physiological two-dimensional (2D) substrates. 2D systems are convenient, allow rapid expansion of biological material and have made important scientific contributions. Nonetheless, their limitations are increasingly acknowledged in biomedical research. Tissue architecture and matrix-mediated signalling are lost, and cells adapt their gene expression in response to the artificial flat surroundings. In response to this, 3D culture models have been engineered to mimic more physiological cellular and/or tissue conditions. Examples are scaffold-free derived matrices, such as collagen gelation or spheroid cell culture (5, 6). Alternatively, scaffold-based 3D techniques include protein-based structures, such as the extensively used Matrigel®, but also natural and synthetic hydrogels and hard polymer scaffolds (7-12). In these systems, cells are seeded on an acellular matrix, polymeric materials or dispersed

in a liquid matrix followed by polymerization. More specific tissue-oriented approaches are 3D bioprinting designs and organ-on-chips (13-15).

In this context, some studies have addressed the development of 3D cultures to study synovial pathophysiology. These are considerably more specialized because of the distinct anatomical characteristics of the synovium, and because SFs in the arthritic joint tissue contain unique features that are not shared by fibroblasts found in other locations, such as hypoxia, substantial inflammatory cell infiltration and distinct matrix remodeling.(16-18) In fact, although expanded SFs preserve epigenetic modifications associated to a pathogenesis,(19) prolonged culture of SFs on 2D surfaces results in a gradual loss of disease phenotype (20, 21). Three-dimensionality in the synovium governs SFs-matrix-dependent signaling, determining the changes in cellular shape and adhesion that contribute to the formation of the pannus, the abnormally thickened synovial tissue that migrates across the articular cartilage and bone causing tissue damage (17). Ex vivo synovial explants have been used as a surrogate of tissue for in vitro studies, although tissue availability from early disease stages is limited and other samples from surgery are too damaged and have been exposed to drugs for years, disturbing basic immune mechanisms. Initial 3D cultures for SFs were conducted 25 years ago in fibrin gels (22), but it is only recently that more diverse methods have been developed. Matrigel-based systems, often described as micromasses, are the most common approach. Matrigel provides a more physiological platform, allowing in vitro differentiation of the lining synovial membrane and SF responses to cytokines such as TNF (7, 23-27). On the other hand, limitations in Matrigel cultures are known, like batch-to-batch variability and undefined composition. Attempts have been made to develop other platforms, either alone or in combination with other synovial cells. These include microfluidic chips incorporating fibrin gels (28), 3D printed collagen/alginate gels (29) or collagen gels (30). In most cases, the choice of the 3D culture and material is determined by the specific biological process to be tested in vitro, such as migration, invasiveness, leukocyte migration or modulation of angiogenesis. But the effect of the culture system on the activation of cellular pathways and SF-dependent inflammation is normally overlooked. Furthermore, given the high degree of variability in the methods found in the literature and differences in composition in Matrigel lots, it is not possible to compare independent results. Thus, how differential culture conditions impact on SF cell biology, outside of the primary experimental readout is often unknown, despite the potential for these effects to directly affect the experimental results generated.

In this study, we use a murine model of arthritis to investigate the influence of ex vivo culture conditions on activated SFs. To provide a broader and integrative perspective, we show a direct

comparison between freshly isolated SFs from the synovium, both from healthy and inflamed joints, and we compared the activated phenotype with cells expanded in conventional 2D cultures and in two unrelated 3D systems: i) fibronectin-(FN)-coated polystyrene scaffolds and ii) fibronectin-(FN)-based 3D hydrogels. Scaffolds were commercially available from Alvetex®, and hydrogels were produced in-house, functionalizing the FN protein with PEG-maleimide (PEGylation) as described before (31). Our results provide a systematic comparison of the transcriptomic signature in healthy and inflammatory SFs expanded in 2D culture and also following transfer to two distinct 3D systems, allowing a reliable understanding of the effect of the culture microenvironment on fibroblast responses. Whilst culture on 2D resulted in a loss of functional phenotype, we discovered that on scaffolds, perhaps mimicking the joint/bone environment, the cells partially recovered their pathogenic phenotype indicating that this may provide a more suitable platform for candidate drug screening. Intriguingly, we found their culture in hydrogels to induce a non-inflammatory or "remission-like" phenotype that may offer therapeutic potential.

Results

Characterization of healthy and activated SFs in 2D culture. We used the murine model of Collagen-Induced Arthritis (CIA), a well-defined and reproducible setup to mimic the SF activation observed in human RA (32). We expanded SFs from both healthy and CIA synovium until passage 3-4, a time point until which we have previously shown CIA SFs to maintain epigenetic changes (33). The cells expressed the stromal marker vimentin and showed the expected flattened morphology, where cell adhesions are restricted to x-y plane, presenting an apical-basal polarity (Figure 1A). Confirming their imprinted pro-inflammatory phenotype, cultured CIA SFs showed elevated IL-6 and Ccl2 production compared with cells expanded from healthy animals and this pathogenic signature was further enhanced in response to IL-17 stimulation in vitro (Figure 1B). SFs are a heterogeneous population, where distinct subsets are found in specific anatomical areas, lining and sublining membrane, and can be identified by $CD90^{-}VCAM^{+}$ and $CD90^{+}VCAM^{-}$ phenotypes respectively (34-36) with non-overlapping functions in the synovium (37, 38). In our model, SFs directly isolated from the joint (not cultured) were mostly sublining $CD90^{+}VCAM1^{-}$ (~70%, Figure 1C), representative of the major population also described in humans (16). A smaller subset (~5%) was identified as $VCAM\text{-}1^{+}$, an adhesion molecule enriched in lining areas and up-regulated in tissue-destructive SFs (16,

35). On the other hand, when SFs were expanded in 2D, they presented a non-physiological phenotype dominated by CD90 and VCAM co-expression (~60-70%, Figure 1D), which represents only a marginal population in vivo and hence such cultured SFs reflect the artefactual enrichment/rewiring of physiologically-relevant functional phenotypes. Yet, both non-cultured and cultured CIA cells increased VCAM1 expression compared to their naïve counterparts, suggesting some preservation of cell activation reflective of that occurring in the arthritic joint. As the artificial $CD90^{+}VCAM1^{+}$ phenotype could be a consequence of the lack of supportive matrix, we coated culture plates with fibronectin (FN) to assess the potential impact of cell-matrix interactions on such SF-mediated inflammatory responses. We selected FN as a model because it accumulates in areas of SF proliferation in RA, guiding SFs to the pannus and up-regulating MMPs through α5β1 and αvβ3 integrin signalling (39, 40). Confirming the association between FN-enriched areas and local inflammation, the presence of FN increased IL-6 and MMP3 expression, an effect that was enhanced in CIA cells (Figure 1E).

2D culture induces fundamental changes in SFs transcriptome. Results in Figure 1 showed that even when SFs expanded in culture preserve some of the inflammatory characteristics of in vivo activated cells, they also undergo extensive phenotypic changes. This was however expected, but it confirmed the influence of cell culture on SFs. Therefore, we decided to conduct a deeper analysis using Next-Generation Sequencing (NGS). First, we utilized our RNA-Seq dataset from SFs directly purified from mouse synovium [GEO Series accession number GSE162306 (41) as a physiological reference of SF activation in arthritis. In this dataset, naïve and arthritic SFs were sorted by FACs ($Podoplanin^{+}CD31^{-}CD45^{-}$) and RNA was immediately purified for sequencing (Figure 2A). The distinction between naïve and CIA cells was quantified by PCA analysis (Figure 2B). Here, 298 genes were up-regulated and 88 genes were down-regulated in arthritic SFs relative to naïve cells (Figure 2C, supplementary Table 1). To generate a detailed molecular and biological reference, we conducted a new functional enrichment analysis on up-regulated genes in CIA SFs integrating KEGG pathways, WiKiPathways and CORUM databases using the bioinformatic tool ClueGO (42). This confirmed SF activation, dominated by enriched functional nodes containing cytokine signalling (IL-17 and TNF), JAK-STAT signalling and cell cycle activation (Figure 2D), in line with the expected arthritic phenotype. To further illustrate this, we designed four gene lists to provide a tailored analysis of mechanisms of known importance for SF-mediated immunopathology which will be relevant for comparison with ex vivo 2D and 3D cultures: i) proliferation, ii) matrix remodeling, iii) secretion

of inflammatory mediators and iv) migratory response (37, 43, 44) (Figure 2E). As expected, all selected genes were up-regulated in activated CIA SFs.

Next, we assessed the transcriptomic signature of arthritic SFs following ex vivo expansion in 2D. We digested mouse synovium as in Figure 2A, but cells were expanded in conventional polystyrene flasks (3-4 passages) prior to culturing them for 7 days on FN-coated surfaces (Figure 2F). RNA was then extracted for RNA-Seq analysis. Like in the non-cultured SFs, PCA still separated both groups (Figure 2G), but the number of differentially expressed (DE) genes in CIA cultured SFs was considerably reduced (112 up-regulated, 12 down-regulated, Figure 2H, Supplementary Table 2). Enrichment analysis showed the loss of inflammatory signature, as well as the cell cycle and proliferation markers from non-cultured cells. Only ECM-receptor interaction, Wnt signalling and adipogenesis were significantly enriched (Figure 2I), although some inflammatory markers like Mmp3, Mmp9, Cxcl13 or Ccl11, and some migration genes, Postn, Cdh11, were still up-regulated, albeit statistical significance was not reached (**Figure 2J**), perhaps sustaining the core for some 'inflammatory memory'. Overall, cells in 2D lost the inflammatory phenotype when compared with "in vivo" cells, despite the presence of FN (figures 2D-E vs 2I-J). Regarding cell migration, even when some genes were differentially expressed in CIA cells, some others showed an opposite regulation compared to the in vivo reference, like Collagen triple helix repeat containing 1 (Cthrc1) (Figure 2E,J), a protein enhancing SF migration in arthritis (45).

Cultured SFs recover their pro-inflammatory phenotype in 3D scaffolds. Our data indicated that the inflammatory phenotype of SFs is largely absent or changed upon 2D culture, along with their cell morphology and differentiation. Because morphology can influence function, signaling and cytokine synthesis (46), we subsequently cultured the expanded SFs in 3D environments in an aim to provide a more physiological environment. We first used commercially available Alvetex® scaffolds made of porous cross-linked polystyrene (47). These are engineered to a thickness of 200 µm with pores around 36-40 µm, with a 'sponge-like' appearance (48). Like in 2D cultures, we coated the scaffold with full-length FN. Scaffolds supported SFs attachment, cell viability and proliferation, as shown by hematoxylin/eosin staining (Figure 3A). SF attachment and distribution within the scaffolds were impacted by interaction with FN, as cells cultured in the presence or absence of FN showed a distinct migratory pattern (Figure 3B). SFs expressed the stromal marker vimentin (Figure 3C), and reconstruction of Z-stacked confocal images stained for phalloidin revealed the SFs to display 3D morphology and rounder more physiological shape (Figure 3C).

Next, we conducted RNA-Seq studies as before to investigate how the new 3D culture conditions impacted on the transcriptome of arthritic SFs. We used the same cells expanded in 2D but transferred them to scaffolds for 7 days prior to RNA isolation and sequencing (Figure 4A). PCA confirmed again the stable nature of distinct naïve and arthritic phenotypes (Figure 4B). Interestingly, in contrast to the low numbers of DE genes observed in 2D conditions, SFs switched to scaffolds showed 548 up-regulated genes and 203 downregulated genes in arthritis relative to naïve SFs (Figure 4C, Supplemental Table 3). Similar pathway analysis showed that many inflammatory pathways were significantly enriched, contained in an organized network sustained by "IL-17 signaling" and "Cytokines and Inflammatory response' terms (Figure 4D), networks reminiscent of those results observed with arthritic SFs purified from joints prior to any cell culture (Figure 2D). Likewise, networks directly involved in cell cycle were detected, in line with the hyperproliferative status of activated SFs in arthritis. Targeted analysis confirmed the recovery of a proliferative and inflammatory signature in arthritic SFs (Figure 4E), whereas matrix remodeling and migration pathways were only partially retrieved and the migration-related Cthrc1, ST3Gal4 and Loxl2 genes displayed a non-physiological regulation (Figure 4E). Collectively these data indicate that the inflammatory phenotype lost in 2D can be at least partially recovered when SFs are transferred to 3D FN-coated scaffolds.

To corroborate these results scaffold at the protein level, we evaluated the expression of the proliferation marker Ki67 by immunofluorescence. CIA SFs in scaffolds showed an elevated proportion of Ki67^{+} cells relative to healthy cells (Figure 4F), confirming the reappearance of the hyperproliferative phenotype of arthritic SFs. Regarding inflammatory mediators, IL-6 and MMP3 secretion in arthritic SFs was up-regulated (Figure 4G). Finally, we evaluated CD90 and VCAM-1 expression by immunofluorescence to define differentiation of SFs into functional subsets. Interestingly, scaffold cultures reduced the percentages of 2D-associated CD90^{+}VCAM-1^{+} co-expression. Only ~20% in naïve and 40% in CIA cells were found to be double positive for these markers (Figure 4H), compared with 65% and 74% of cells in 2D (Figure 1D) and 2% and 6% in vivo (Figure 1C). Thus, scaffolds 'reversed' 2D SFs artefactual differentiation towards a more physiological phenotype in terms of proliferation, production of inflammatory factors and subset differentiation.

FN-based hydrogels drive arthritic SFs towards a non-inflammatory phenotype. ECM-derived matrices are relatively common in rheumatology research to study SF migration. Matrigel (49) obtained from Engelbreth-Holm-Swarm mouse sarcoma dominates the current literature, but it may not offer an ideal system to study the role of matrix in inflammation because

of its undefined composition and batch variability. Furthermore, the effect of a gel-based structure on SF activation is usually overlooked. To address this, we used engineered hydrogels containing full-length FN as the only matrix component to study its influence on SF-mediated inflammation within a gel structure. Full-length FN was functionalised with poly(ethylelene) glycol (PEG)-maleimide (PEGMAL), allowing covalently crosslinking within a synthetic network to create a 3D FNPEG gel (31). We first investigated whether hydrogels supported SF viability. SFs were expanded in 2D until passages 3-4, after which they were incorporated into hydrogels. Expression of the stromal marker vimentin was maintained (Figure 5A). Intriguingly, cells showed an unexpected tropism and relocated towards the hydrogel edge (Figure 5A). We observed a survival rate of 70-80% after 14 days in culture (Figure 5B).

Then, we conducted RNA-Seq studies, in line with the experiments done for 2D and scaffolds. To extract RNA, hydrogels needed to be degraded, so a protease-degradable VPM peptide (GCRDVPMSMRGGDRCG) (50) was incorporated in the network. Such chemical modification does not affect the mechanical or structural properties of FNPEG hydrogels (31). Cells expanded in 2D were integrated in hydrogels and RNA was isolated at day 3 of culture (Figure 6A) because longer time points resulted in gel degradation and consequent cell loss, probably because of their constitutive secretion of MMPs. PCA confirmed the distinct profile of naïve and arthritic SFs (Figure 6B). DE genes in arthritic SFs relative to naïve were identified, showing 112 genes upregulated and 67 downregulated (Figure 6C, supplementary Table 4), numbers lower than those seen with scaffolds or non-cultured cells and more akin to those observed in 2D. Surprisingly, not only the number of up-regulated genes was low in arthritic SFs, but the pathways associated with such gene expression were not reflective of inflammatory cells either. Rather, pathway enrichment revealed a significant regulation of ECM-receptor interaction and tissue remodelling genes and pathways (Figure 6D). In fact, targeted analysis of arthritogenic pathways indicated that arthritic SFs in hydrogels decreased expression of such proliferation and inflammatory markers and showed an opposite pattern of migratory gene expression compared with the original arthritic cells (Figure 6E). Interestingly, MMPs were still up-regulated, supporting the induction of matrix and tissue remodeling pathways in hydrogels.

To validate the biological effect observed in hydrogel culture, we collected culture supernatants to analyze MMP3, IL-6 and Ccl2 expression using degradable hydrogels, as in the RNA-Seq experiments (Figure 6F). MMP3 expression was significantly higher in arthritic SFs, confirming RNA-Seq data. IL-6 and Ccl2 were also higher in CIA SFs, differing from the transcriptomic results. This could be explained by the higher expression of MMPs in arthritic SFs, meaning that

arthritic SFs could degrade the gel quicker, which may allow release of cytokines to the media. By contrast, naïve SFs would not degrade the gel because of the low MMP expression, resulting in no release of cytokine outside the gel boundaries. This hypothesis is supported by experiments done in hydrogels lacking VPM peptide, and therefore non-degradable and resistant to MMP degradation (Figure 6G). In such non-degradable gels, cytokine levels in supernatants were lower than in degradable gels, and arthritic SFs showed similar, or even lower expression of inflammatory cytokines. This reflects a reduction of the inflammatory capacity of arthritic SFs when switched to hydrogels, in agreement with our transcriptomic results. Next, we evaluated cell distribution within the gels. Cell nuclei were stained with DAPI, hydrogels were fully scanned and reconstructed in 3D images (Figure 6H). We measured the distance of single cells to the image border, as a surrogate value for cell migration within the gel. No difference was observed between naïve and CIA cells (Figure 6H), indicating that arthritic SFs do not have a distinct migration or adhesion signature in hydrogels and suggesting again a loss of pathogenic pathways associated with chronic disease. Finally, we stained for CD90 and VCAM1 to evaluate subset specialization. Following scanning of the full gel, we did not find a clear $CD90^{+}VCAM-1^{+}$ phenotype (Figure 6I) as seen in 2D, although we were not able to quantify double positive cells due to technical limitations of the imaging software. However, in naïve cells the number of $CD90^{+}$ cells was significantly higher than those expressing VCAM1, suggesting the absence of the dominant $CD90^{+}VCAM1^{+}$ phenotype observed in 2D.

Our results showed that whilst scaffolds represent a valuable system to better maintain the SF inflammatory phenotype in vitro, hydrogels redirect pathogenic fibroblasts towards a tissue remodeling and non-inflammatory phenotype, conclusions corroborated in a multisystem comparison using Metascape (51) (Figure 7). Identification of DE genes shared among systems corroborated the similarities between in vivo SF activation and scaffold cultures, with hydrogels being the most distinct group (Figure 7A). This was supported by an integrative analysis of Canonical Pathways, KEGG pathways and WiKi pathways (Figure 7B), showing hydrogels being the only system that did not show enriched IL-17-mediated pathways, a hallmark of inflammatory arthritis. This highlights the rewiring effect of 3D hydrogels on SF, a process that increased transcriptional activity of TWIST2 and decreased Jun and YBX1 (Figure 7C).

SF responses to IL-1β stimulation in 2D and 3D in vitro systems. To evaluate how stable the hydrogel-dependent rewiring of SFs was, we evaluated whether healthy cells responded to exogenous inflammatory stimulation using IL-1β. This induced activation in 2D, scaffolds and hydrogels systems, up-regulating inflammatory cytokines and chemokines Csf3, IL-6, or Ccl2

(Figure 8A, supplementary Table 5). Interestingly, although SFs cultured in hydrogels still responded to IL-1β stimulation, the response was significantly less strong than in SFs from the other platforms. For example, fold increase for Csf3 was 273 in 2D, 3816 in scaffolds and only 15 in hydrogels (Supplementary Table 5). The ability to prevent inflammation of hydrogels was further evidenced by their reduced number of up-regulated genes (Figure 8B) and enriched pathways (Figure 8C) upon IL-1β stimulation. Mechanistically, IL-1β failed to induce expression of genes regulated by the transcription factors HIF1A, ESR1, STAT6 and SMAD3 (Figure 8D) in hydrogels, but not in 2D and scaffolds, reflecting the less inflammatory environment found in hydrogels.

Discussion

Our results show a critical loss of the pathophysiological phenotype of inflammatory SFs expanded in 2D. This results were expected and confirm previous observations (20, 21). However, we demonstrate that the loss of inflammatory phenotype is not permanent and can be retrieved when the right environmental conditions are provided. Relocation of 2D SFs into scaffolds restored a significant number of pathogenic pathways, whilst perhaps surprisingly, FNPEG hydrogels pushed arthritic cells towards a non-inflammatory and remodeling phenotype. This reveals that SFs retain a high degree of plasticity such that their phenotype is ultimately determined by ongoing signals coming from the microenvironment. Because such signals can be recapitulated by biomaterials, our findings can impact in two major areas of research, i) development of more physiological 3D culture methods to study SF biology and ii) discovery of novel approaches to modulate fibroblast-mediated inflammation in chronic disease.

Regarding culture methods for SFs, our findings in rigid scaffolds may lead to more physiological and affordable systems able to support pathophysiological matrix-dependent signaling and interactions. Major advances in drug discovery for RA have been made over the last decade (52, 53). Yet, as the therapies available all target immune system cells and inflammation, they are subject to immunosuppressive side-effects that would be avoided with drugs targeting the fibroblast compartment. However, despite increasing knowledge of the role that SFs play in the perpetuation of disease, this information has not been successfully translated from the pre-clinical to clinical stage. One reason for this could be that in vitro assays for drug screening do not accurately recapitulate the synovial 3D space and associated signaling, preventing identification of relevant targets. Consistent with this, our data show that the culture

conditions determine the transcriptomic and functional phenotype of SFs. The hyperproliferative and inflammatory signature of arthritic SFs is lost in 2D expanded SFs, even when epigenetic changes alter cell function and apparently stably imprint SFs (54-57). Such epigenetic regulation includes DNA hypomethylation and microRNA expression. The methylation pattern in RA SFs is stable over many cell passages in 2D, but these cultured cells still show a non-physiological phenotype. Interestingly, dysregulated epigenetic pathways in arthritic SFs are related to cell cycle, cell adhesion, immune function, and cytokine signaling (33). Such pathways define a phenotype that is lost in 2D but recovered in FN-coated 3D scaffolds, suggesting that cell morphology and environmental cues and signaling are also required to establish and maintain the epigenetically imprinted inflammatory program. This could also explain why RA affect only some joints, and why DNA methylation and transcriptomic SF patterns differ between joints (58).

Thus, it is essential to establish routine culture conditions to mimic the joint microenvironment in vitro, identifying the right structure and materials. This is especially important for samples collected at early disease stages, where the availability of biological tissue is very low and the accuracy in the diagnosis, such as disease phenotype, can be critical to start efficient treatment and to prevent irreversible tissue damage. Culture of SFs from individual patients in 3D scaffolds would allow better patient stratification and drug screening, as it could preserve the SF-dependent pathophysiology during in vitro diagnostic methods. Our study supports this hypothesis, but follow-up studies in the human context are required to validate this. Ultimately, an in vitro synovium model should consider inclusion of other cell types known to interact with SFs to create the synovial environment. Mondadori et al (28) designed a microfluidic chamber to model multi-cellular interactions, including synovial and cartilage compartments to mimic SF-chondrocyte-monocyte interactions. Similarly, Peck et al addressed the same problem, using a tri-culture platform and cell lines to model SFs and macrophages(59) whilst 3D systems to co-culture SFs and endothelial cells have been used to study cell migration and growth factors (29, 30). The results from these studies will be important towards the final aim of generating a synovium-on-a-chip system, although a comparative analysis of the results found in the literature may not be possible given the technical diversity employed. Currently, most research in 3D SF culture have focused on hydrogels of various nature, Matrigel being the most common choice, but also employing fibrin, collagen or alginate hydrogels. 3D hydrogels are generally used to study specific cellular responses, such as cell migration, but the effect of the culture system on global SF responses is often neglected. Our results reveal that hydrogels not only failed to restore

the hyperproliferative and inflammatory signature in arthritic SFs, but they rewired the already activated cells towards an altered phenotype, closer to a remission-like phenotype and distant from the original inflammatory phenotype in vivo. Matrigel has been shown to enhance expression of MMPs in RA SFs without affecting IL-6, and to allocate cells at the edge of the cells (7, 24), in agreement with our results in FN hydrogels. This could indicate that mechanical properties found in gel-like structure could facilitate the formation of distinct anatomical structures. Such structures have elegantly revealed novel physiological roles for Integrin α9 and Cadherin-11(7, 24), but deeper analysis are needed to fully understand how close gel systems are to synovial tissues. In this work, arthritic SFs cultured on hydrogels showed significantly up-regulated pathways involved in osteogenesis, tissue remodeling and decreased cytokine/chemokine secretion. This difference with the rigid 3D scaffolds highlights the relevance of the culture method in SF-dependent responses. This should be considered in the design of 3D systems to mimic the arthritic synovium, but it also offers new avenues for therapeutic intervention, since this demonstrates that inflammatory SFs can be reprogramed. Several factors could explain the differences observed in our models. Although in our study we always started with FN-based environments, distinct matrisomes can be formed. Our RNA-Seq data showed that 2D cells simply lose most of the inflammatory factors, but arthritic SFs in hydrogels actively up-regulate genes not seen in 2D, nor in rigid scaffolds: for example, collagen fibrils biosynthesis and crosslinking (collagen alpha chains Col1, Col3, Col4, Col6, Col12, *P4ha*, *Adamst2*) and elastic fibre formation (Combining fibronectin, fibulins and microfibrillar-associated proteins) pathways. This could establish pro- or anti-inflammatory fibroblast-matrix crosstalk, events that contribute to RA progression at early disease stages via TLR4 signaling.(60) Moreover, the properties of materials for tissue culture influence FN conformation and integrin binding(61, 62) and functional growth factor presentation (63), which can influence cellular processes like cell migration, integrin activation and subsequent inflammatory responses. Ultimately, the culture system could affect their cell subset specialization, such as lining and sublining fibroblast, that drive tissue damage and inflammation respectively (16). This hypothesis could open new bioengineering solutions, since we could combine materials to reproduce different synovial anatomical locations in vitro.

Nevertheless, the factors driving FN-dependent rewiring are still unclear and require further investigation. Differences in the stiffness of scaffolds and hydrogels suggest that this could be an important aspect to consider, and it is one limitation in our study. In fact, the arthritic joint is known to increase the stiffness of the synovium above normal values(64). Differential

mechanical forces in the joint could therefore be the required signal for SFs to start inflammatory circuits, something that could involve interactions with FN and other matrix components. Additionally, our study is restricted to fibronectin-based systems, which we used as a model of SFs enriched areas, but the synovial matrix is formed by many other components that are likely to play a role in SF-biology and disease progression. This should be considered in future studies to understand basic fibroblast pathology and to develop relevant in vitro models. Thus, recapitulation of homeostatic and inflammatory environments should be fully understood in order to develop novel in vitro systems and even therapeutic opportunities, not only in RA, but in other chronic inflammatory conditions where fibroblasts-matrix interactions play a role in disease progression. Our results highlight the importance of the culture system in the outcome of in vitro experiments, paving the way for a more rational use of these tools in rheumatology research, as well as new clinical approaches to reconfigure arthritic SFs towards a resolving anti-inflammatory phenotype.

Methods

Mice and Collagen-Induced Arthritis (CIA) model. Male DBA/1 mice were purchased at 8 weeks of age (Envigo; Bicester, UK) and then housed and maintained at the Central Research Facility in the University of Glasgow. All experiments were approved by and carried out in accordance with the Animal Welfare and Ethical Review Board of the University of Glasgow, UK Home Office Regulation and Licenses PPL P8C60C865 and PIL ID5D5F18C. CIA was induced using bovine Collagen type II (100 µg) emulsified with complete Freud's adjuvant (MD Biosciences) and injected intradermally on day 0. On day 21, mice were injected intraperitoneally with a further 200 µg of collagen in PBS. Inflammation of paws was assessed every 2 days through an articular scoring system and the use of a calipers to measure paw width. Joint pathology was scored as follows: 0 = No evidence of erythema or swelling, 1 = Erythema and mild swelling confined to tarsals or ankle joints, 2 = Erythema and mild swelling extending from the ankle to the tarsals, 3 = Erythema and moderate joint swelling extending from the ankle to metatarsal joints, 4 = Erythema and severe swelling encompassing ankle, foot and digits or ankyloses of the limb. Mice were culled once stable pathology was established, typically between day 31 to day 35. A total articular index of 10 or more, paw thickness exceeded 4.5 mm or weight loss exceeded 20% of controls were considered immediate experimental endpoints.

Ex vivo expansion of SFs from murine joints. For isolation and culture of SFs, hind and front paws were harvested from mice, skin and soft tissue were removed, followed by washing 2 times

in 70% ethanol and DMEM medium containing antibiotics (1% penicillin and streptavidin) before dissection. Samples were transferred paws to DMEM containing 10% FCS, 1% antibiotics, 1% nystatin, 1% glutamine and 1mg/ml type II collagenase (Sigma). 1 mg/ml DNase I (Sigma) was added for FACs experiments. Samples were incubated with constant shaking at 37°C for 80 min. After digestion, EDTA was added at a final concentration of 0.5mM and incubated at 37°C for 5 min. Following completion of the incubation time, samples were vortexed vigorously to release cells. Cells were then centrifuged, and supernatant was discarded. For cell expansion, cells were resuspended in complete DMEM medium (10% FCS, 1% penicillin and streptavidin, 1% L-glutamine and 1% non-essential aminoacids) and seeded in culture flasks. Culture medium was refreshed after 24 hours. Cells were fed twice a week and passaged when they reached 90% confluence using trypsin EDTA (ThermoFisher Scientific). Cultured cells were used at passage 3 or 4. Cultured cell purity was accessed by flow cytometry before experiments, CD11b+ cells were removed using magnetic column. Phenotype was evaluated following trypsinization by Flow Cytometry using anti-mouse podoplanin (PDNP)-alexa 647, anti-mouse CD11b-FITC, anti-mouse CD90PECy7 and anti-mouse VCAM-1-FITC antibodies. Zombie Violet dye (Biolegend) was used to exclude dead cells from analysis. All antibodies were purchased from eBioscience. For *in vitro* stimulation of SFs, recombinant IL-1β and IL-17 (immunotools) were used at 10 ng/ml for 12 hours to measure cytokine release by ELISA or 6 hours for transcriptomic experiments.

Culture of expanded SFs in Alvetex® scaffolds. Alvetex® scaffolds (AMS Biotechnology (Europe) Lt, Abingdon) were rendered hydrophilic with 70% ethanol. The ethanol was removed, and the scaffolds washed with PBS twice (for ~1 min) and aspirated. The scaffolds were then coated with fibronectin (RD System, 1030-FN) in PBS (0.5 mg/ml) and incubated at room temperature for 1 h in a well plate. The FN solution was then aspirated and replaced with complete DMEM medium. Scaffolds were then seeded with cells (1 x 10^6 cells per 6-well plate scaffold), with the cells dispensed at the centre of the scaffold and then incubated at 37°C, 5% CO_2 for 2 h to facilitate cell attachment. The cells were then gently flooded with cDMEM medium and cells were then grown on the scaffold for the indicated days, with the medium being replaced every second day.

Preparation of FNPEG hydrogels. FNPEG hydrogels were prepared as previously described (31), following the subsequent steps: 1- Denaturation of FN. Fibronectin (FN) (YoProteins, 3 mg mL^{-1}; 50 µg per 50 µl hydrogel) was pegylated. FN was denatured in 100 µl denaturing buffer (5 mM Tris(2-carboxyethyl)phosphine hydrochloride [TCEP, pH 7, Sigma] and 8 M urea

[Fisher, 18 M stock] in phosphate buffer saline [PBS, Gibco, pH 7.4]) for 15 min at room temperature. 2- Protein PEGylation. An appropriate amount of 4-arm-PEG-Maleimide (PEGMAL, LaysanBio) was incubated for 30 min at room temperature at a molar ratio FN:PEGMAL 1:4. The tubes were then placed on a rotating platform (100 rpm) at room temperature for 30 min. The reaction was stopped with 0.5 µl NaOH at 1M. 3- Protein alkylation. The remaining non-reacted cysteine residues were blocked by alkylation using 14 mM iodoacetamide (IAA, Sigma) in PBS at pH 8 (on a rotating platform (100 rpm)) for 2 h at room temperature. The product of the reaction was dialysed (Mini-A-Lyzer, MWCO 10 KDa, ThermoFisher) against PBS for 1 h at room temperature. 4- Protein precipitation. Nine volumes of cold absolute ethanol were added to the protein solution and mixed well using a vortex mixer. The mixture was then incubated at −20°C overnight and centrifuged at 15,000 g and 4°C for 15 min. The supernatant was discarded, and the protein pellet was further washed with 90% cold ethanol and centrifuged again at 15,000 g and 4°C for 5 min. Pellets were dried and solubilized using 8 M urea at a final protein concentration of 2.5 mg/mL. Once the protein was dissolved, the solution was dialysed against PBS for 1 h and stored in the freezer. 5- Hydrogel formation. PEG hydrogels were formed using the Michael-type addition reaction under physiological pH and temperature. Briefly, a final concentration of 1 mg/mL of PEGylated FN was added to PEGMAL. Following this, the thiolated crosslinker was added, at a molar ratio 1:1 maleimide:thiol to ensure full crosslinking. The crosslinkers used were either PEG-dithiol (PEGSH, 2 kDa, Creative PEGWorks; for non-degradable gels) or mixtures of PEGSH and protease-degradable peptide (VPM peptide, GCRDVPMSMRGGDRCG, purity 96.9%, Mw 1696.96 Da, GenScript; for degradable gels). SFs were mixed with the protein and PEGMAL before addition of the crosslinker. To allow gelation, samples were incubated for 1 h at 37 °C once the crosslinker was added. Hydrogels were 5% FNPEG with 0.5% VPM for degradable gels.

RNA extraction and RNA-Seq. RNA from cells in 2D and scaffold cultures were extracted using RNeasy MiniElute spin columns (Qiagen) according to manufacture's instructions at the indicated times. RNA was extracted from degradable hydrogels containing VPM and lacking PEGSH. After 3 days in culture, the hydrogels were removed from their inserts and placed in tubes with an equal volume of 2.5 mg/ml collagenase in PBS and incubated at 37ºC for 90 min, gently pipetting samples slowly every 30 min to help release cells. Following incubation, the samples were pipetted vigorously and passed through 100 µm cell strainers into tubes and then centrifuged at 500 g for 10 min at 4ºC. RNA was extracted using Qiagen kit, as per manufacture

instructions. RNA integrity was checked using the Agilent 2100 Bioanalyzer System. Samples with a RIN value >9 were used for further experiments. For 2D and Alvetex® samples the libraries were prepared using the TruSeq mRNA stranded library preparation method. For FNPEG hydrogels the libraries were prepared using the NEBNext Single Cell-Low Input RNA Library Prep Kit for Illumina. All samples were sequenced 2 × 75 bp to an average of more than 30 million reads. RNA-Seq reads were then aligned to the mouse reference genome (GRCM38) using Hisat2 version 2.1.0, and featurecounts version 1.4.6 was used to quantify reads counts using the Galaxy portal (University of Glasgow). Data quality control, non-expressed gene filtering, median ratio normalization (MRN) implemented in DESeq2 package, and identification of differentially expressed (DE) genes was done using the R Bioconductor project DEbrowser (65). Genes that passed a threshold of padj < 0.01 and log2foldChange > 2 in DE analysis were considered for further analysis. The Cytoscape (66) plug-in ClueGO (42) was used for analysis and visualization of enriched pathways in DE genes. Gene ontology terms from KEGG pathways, Wikipathways and CORUM were used to analyze enriched pathways and group functionally related networks. Metascape software (51) was used for multi-system comparisons in the generation of circos plots and identification of statistically enriched terms in GO/KEGG terms, wikipathways, GSRA and GO_TRRUST.

Immunohistochemistry of scaffolds and hydrogels. For preparation of scaffold blocks and sections, culture medium was aspirated after culture at indicated times and washed 3 times with cold PBS. The scaffolds were then removed from their inserts and fixed with 4% PFA at 4ºC for 12h. The fixative was aspirated, and the scaffolds were washed with PBS and dehydrated using a series 30%, 50%, 70%, 80%, 90% and 95% solutions of ethanol, 15 min each, and 100% absolute ethanol for 30 minutes. Scaffolds were embedded using a Lecia Asap 300 processor (Histoclear [Merk] 30 min, 50:50 solution of Histoclear:paraffin wax 50:50 ratio 60 °C for 30 min and Histoclear:paraffin wax mix 60°C for 60 min). The wax was left to cool and set at room temperature for 2 hours. Sections were cut at 7 µm thickness for further analysis. Hydrogels were fixed in 4% PFA for 30 min, following Hydrogels dehydration in 30% sucrose solution in PBS overnight at 4ºC and subsequently embed in Tissue-Tek® O.C.T. compound (Sakura). Samples were placed immediately at -80ºC overnight prior to cutting sections at 20 µm.

Immunofluorescence. For cell staining, SFs (2000-5000) were seeded on a chamber slide and fixed with 4% PFA for 10 min at room temperature. Cells were washed three times with PBS and permeabilized with PBS 0.05% Triton X-100 for 10 minutes and blocked (PBS 1% BSA) for 1 hour. Slides were washed three times in PBS 0.05% Tween 20 (PBS-T) before being

incubated with primary antibody overnight at 4°C. Primary antibodies used were: anti-vimentin (Sigma); anti mouse CD90 (Biolegend), anti-mouse VCAM-1 (eBioscience) and anti-mouse Ki67 (Abcam). Slides were then washed three times in PBS-T and incubated with fluorochrome conjugated secondary antibodies for 2 hours at room temperature. Phalloidin-FITC (Thermofisher Scientific) was used to visualise actin. Slides were mounted with SlowFade™ Diamond Antifade Mountant with DAPI (ThermoFisher Scientific) to stain nuclei and covered with a glass cover slip. Slides were visualized with an EVOS^{TM} FL Auto 2 microscope. For imaging of whole hydrogels, gels were fixed with 4% PFA for 30 min at room temperature. Permeabilisation of the cells was carried out for 15 min at room temperature using 0.1% Triton in PBS, followed by washing once with PBS. The hydrogels were then treated with PBS 1% BSA for 30-60 min at room temperature, after which the primary antibody was added and left overnight at 4ºC. Samples were treated with the appropriate secondary antibody for 1 h at room temperature and washed with PBS 0.5% Tween20 before mounting onto a glass bottom petri dishes using Vectashield slow fade media containing DAPI (VectorLabs). Scanning and imaging was carried out on a Leica DM8 widefield microscope using LAS X Life Science software at a magnification of x10. The hydrogels were imaged in a tilescan format with z-steps of ~10 µm to obtain stacked images, which were then merged. The image was then deconvoluted using Huygens essential after which it was processed using IMARIS ("Cell biologist package") to obtain 3D reconstructions and spacial cell analysis.

Hematoxilin/Eosin staining. For paraffin sections, slides were heated in an oven at 60°C for 35 min to melt wax. Sections were immersed in xylene to dewax and in graded ethanol solution (100%, 90% and 70%) to hydrated. Then washed in running water to remove all reagents. Sections were then stained in Harris Haematoxylin for 2-3 min and washed under running water to remove excess dyes. Staining background was reduced by dipping section in 1% acid for a few second, quickly rinsed in running water, immersed in Scott's Tap Water Substitute for 30 seconds and then quickly rinsed in running water. Counter staining was then carried out by dipping sections in 70% ethanol for 9-10 times and immersed in 1% Eosin for 2-3 min. Sections were then dehydrated followed by immersed in 90% ethanol for 1 min, 100% ethanol for 6 min and 100% xylene for 6 min. Sections were then mounted with DPX mountant and sealed with coverslips. For staining of frozen section such as hydrogels, slides were fixed in ice-cold acetone/ethanol (75%/25%) for 10 min at room temperature, then left to air dry for 10 minutes prior to staining as described for hydrated paraffin samples.

Enzyme-linked immunoassays (ELISA*)*. IL-6, CCL2 and MMP3 secretion was detected using ELISA kit (R&D, Dou set) following manufacturer's instructions. SFs were seeded in 96 well plates (Corning) at 10,000 cells per well in 200 µl cDMEM. For scaffolds, cell number was quantified using crystal violet (Sigma). Cells were stained with 100 µl of crystal-violet (0.04 mg/ml) for 30 min at room temperature, then washed at least three times to remove any residual dye. 1% SDS solution (Sigma) was added next to dissolve cells for 1 hour in a shaker. Absorbance was read at 595 nm using a Tecan Sunrise plate reader.

Flow Cytometry. Cultured cells were detached from the plates by trypsin treatment. Cells were stained with Zombie Violet (Biolegend) or flexible viability dye eFluor 780 (eBioscience) at 1 µl/ml in PBS for 20 min on ice to exclude dead cells. Cells were then washed three times with FACS buffer (PBS with 0.5% FCS and 2mM EDTA), and Fc receptor was blocked using CD16/CD32 specific antibody for 20 min on ice. Primary antibodies used were anti-CD31 (Invitrogen), anti-CD45 (Biolegend), anti-CD90.2 (Biolegend), anti-VCAM-1 (Biolegend) and anti-PDPN (Biolegend). Data were acquired using a BD LSRII flow cytometer and analyzed with FlowJo software 8.7.3.

Statistical analysis. Data are presented as the mean ± standard deviation (SD). Statistical analysis was performed with Prism 8 software (GraphPad). One-way analysis of variance (ANOVA) was used to test for comparing differences among multi-groups, student t-test was used to show differences between two study groups. P values <0.05 were considered significant (*).

References

1. Akhavani MA, Madden L, Buysschaert I, Sivakumar B, Kang N, Paleolog EM. Hypoxia upregulates angiogenesis and synovial cell migration in rheumatoid arthritis. Arthritis research & therapy. 2009;11(3):R64.
2. Lee H-Y, Jeon H-S, Song E-K, Han M-K, Park S-I, Lee S-I, et al. CD40 ligation of rheumatoid synovial fibroblasts regulates RANKL-mediated osteoclastogenesis: evidence of NF-kappaB-dependent, CD40-mediated bone destruction in rheumatoid arthritis. Arthritis and rheumatism. 2006;54(6):1747-58.
3. Araki Y, Tsuzuki Wada T, Aizaki Y, Sato K, Yokota K, Fujimoto K, et al. Histone Methylation and STAT-3 Differentially Regulate Interleukin-6-Induced Matrix

Metalloproteinase Gene Activation in Rheumatoid Arthritis Synovial Fibroblasts. Arthritis & rheumatology (Hoboken, NJ). 2016;68(5):1111-23.
4. Nayar S, Campos J, Smith CG, Iannizzotto V, Gardner DH, Mourcin F, et al. Immunofibroblasts are pivotal drivers of tertiary lymphoid structure formation and local pathology. Proceedings of the National Academy of Sciences of the United States of America. 2019;116(27):13490-7.
5. Nyga A, Neves J, Stamati K, Loizidou M, Emberton M, Cheema U. The next level of 3D tumour models: immunocompetence. Drug discovery today. 2016.
6. Nystrom ML, Thomas GJ, Stone M, Mackenzie IC, Hart IR, Marshall JF. Development of a quantitative method to analyse tumour cell invasion in organotypic culture. J Pathol. 2005;205(4):468-75.
7. Emori T, Hirose J, Ise K, Yomoda JI, Kasahara M, Shinkuma T, et al. Constitutive Activation of Integrin alpha9 Augments Self-Directed Hyperplastic and Proinflammatory Properties of Fibroblast-like Synoviocytes of Rheumatoid Arthritis. J Immunol. 2017;199(10):3427-36.
8. Sarrigiannidis SO, Rey JM, Dobre O, Gonzalez-Garcia C, Dalby MJ, Salmeron-Sanchez M. A tough act to follow: collagen hydrogel modifications to improve mechanical and growth factor loading capabilities. Mater Today Bio. 2021;10:100098.
9. Maji S, Lee H. Engineering Hydrogels for the Development of Three-Dimensional In Vitro Models. Int J Mol Sci. 2022;23(5).
10. Kahraman E, Ribeiro R, Lamghari M, Neto E. Cutting-Edge Technologies for Inflamed Joints on Chip: How Close Are We? Front Immunol. 2022;13:802440.
11. Habanjar O, Diab-Assaf M, Caldefie-Chezet F, Delort L. 3D Cell Culture Systems: Tumor Application, Advantages, and Disadvantages. Int J Mol Sci. 2021;22(22).
12. Benton G, Arnaoutova I, George J, Kleinman HK, Koblinski J. Matrigel: from discovery and ECM mimicry to assays and models for cancer research. Adv Drug Deliv Rev. 2014;79-80:3-18.
13. Witte K, Rodrigo-Navarro A, Salmeron-Sanchez M. Bacteria-laden microgels as autonomous three-dimensional environments for stem cell engineering. Mater Today Bio. 2019;2:100011.
14. Tsuda S, Jaffery H, Doran D, Hezwani M, Robbins PJ, Yoshida M, et al. Customizable 3D Printed 'Plug and Play' Millifluidic Devices for Programmable Fluidics. PLoS One. 2015;10(11):e0141640.

15. Carvalho MR, Barata D, Teixeira LM, Giselbrecht S, Reis RL, Oliveira JM, et al. Colorectal tumor-on-a-chip system: A 3D tool for precision onco-nanomedicine. Sci Adv. 2019;5(5):eaaw1317.
16. Croft AP, Campos J, Jansen K, Turner JD, Marshall J, Attar M, et al. Distinct fibroblast subsets drive inflammation and damage in arthritis. Nature. 2019;570(7760):246-51.
17. Bottini N, Firestein GS. Duality of fibroblast-like synoviocytes in RA: passive responders and imprinted aggressors. Nature reviews Rheumatology. 2013;9(1):24-33.
18. Frank-Bertoncelj M, Trenkmann M, Klein K, Karouzakis E, Rehrauer H, Bratus A, et al. Epigenetically-driven anatomical diversity of synovial fibroblasts guides joint-specific fibroblast functions. Nature communications. 2017;8:14852.
19. Whitaker JW, Shoemaker R, Boyle DL, Hillman J, Anderson D, Wang W, et al. An imprinted rheumatoid arthritis methylome signature reflects pathogenic phenotype. Genome Med. 2013;5(4):40.
20. Hardy RS, Hulso C, Liu Y, Gasparini SJ, Fong-Yee C, Tu J, et al. Characterisation of fibroblast-like synoviocytes from a murine model of joint inflammation. Arthritis Res Ther. 2013;15(1):R24.
21. Zimmermann T, Kunisch E, Pfeiffer R, Hirth A, Stahl HD, Sack U, et al. Isolation and characterization of rheumatoid arthritis synovial fibroblasts from primary culture--primary culture cells markedly differ from fourth-passage cells. Arthritis Res. 2001;3(1):72-6.
22. Schultz O, Keyszer G, Zacher J, Sittinger M, Burmester GR. Development of in vitro model systems for destructive joint diseases: novel strategies for establishing inflammatory pannus. Arthritis Rheum. 1997;40(8):1420-8.
23. Kiener HP, Watts GF, Cui Y, Wright J, Thornhill TS, Skold M, et al. Synovial fibroblasts self-direct multicellular lining architecture and synthetic function in three-dimensional organ culture. Arthritis Rheum. 2010;62(3):742-52.
24. Kiener HP, Lee DM, Agarwal SK, Brenner MB. Cadherin-11 induces rheumatoid arthritis fibroblast-like synoviocytes to form lining layers in vitro. Am J Pathol. 2006;168(5):1486-99.
25. Broeren MGA, Waterborg CEJ, Wiegertjes R, Thurlings RM, Koenders MI, Van Lent P, et al. A three-dimensional model to study human synovial pathology. ALTEX. 2019;36(1):18-28.
26. Rothbauer M, Byrne RA, Schobesberger S, Olmos Calvo I, Fischer A, Reihs EI, et al. Establishment of a human three-dimensional chip-based chondro-synovial coculture joint model for reciprocal cross talk studies in arthritis research. Lab Chip. 2021;21(21):4128-43.

27. Tolboom TC, Huizinga TW. In vitro matrigel fibroblast invasion assay. Methods Mol Med. 2007;135:413-21.
28. Mondadori C, Palombella S, Salehi S, Talo G, Visone R, Rasponi M, et al. Recapitulating monocyte extravasation to the synovium in an organotypic microfluidic model of the articular joint. Biofabrication. 2021;13(4).
29. Lin J, Sun AR, Li J, Yuan T, Cheng W, Ke L, et al. A Three-Dimensional Co-Culture Model for Rheumatoid Arthritis Pannus Tissue. Front Bioeng Biotechnol. 2021;9:764212.
30. Jeffery HC, Buckley CD, Moss P, Rainger GE, Nash GB, McGettrick HM. Analysis of the effects of stromal cells on the migration of lymphocytes into and through inflamed tissue using 3-D culture models. J Immunol Methods. 2013;400-401:45-57.
31. Trujillo S, Gonzalez-Garcia C, Rico P, Reid A, Windmill J, Dalby MJ, et al. Engineered 3D hydrogels with full-length fibronectin that sequester and present growth factors. Biomaterials. 2020;252:120104.
32. Brand DD, Latham KA, Rosloniec EF. Collagen-induced arthritis. Nature protocols. 2007;2(5):1269-75.
33. Corbet M, Pineda MA, Yang K, Tarafdar A, McGrath S, Nakagawa R, et al. Suppression of inflammatory arthritis by the parasitic worm product ES-62 is associated with epigenetic changes in synovial fibroblasts. PLoS Pathog. 2021;17(11):e1010069.
34. Edwards JC. Fibroblast biology. Development and differentiation of synovial fibroblasts in arthritis. Arthritis Res. 2000;2(5):344-7.
35. Croft AP, Naylor AJ, Marshall JL, Hardie DL, Zimmermann B, Turner J, et al. Rheumatoid synovial fibroblasts differentiate into distinct subsets in the presence of cytokines and cartilage. Arthritis research & therapy. 2016;18(1):270.
36. Wu Z, Ma D, Yang H, Gao J, Zhang G, Xu K, et al. Fibroblast-like synoviocytes in rheumatoid arthritis: Surface markers and phenotypes. Int Immunopharmacol. 2021;93:107392.
37. Mizoguchi F, Slowikowski K, Wei K, Marshall JL, Rao DA, Chang SK, et al. Functionally distinct disease-associated fibroblast subsets in rheumatoid arthritis. Nature communications. 2018;9(1):789.
38. Zhang F, Wei K, Slowikowski K, Fonseka CY, Rao DA, Kelly S, et al. Defining inflammatory cell states in rheumatoid arthritis joint synovial tissues by integrating single-cell transcriptomics and mass cytometry. Nature immunology. 2019.
39. Lowin T, Straub RH. Integrins and their ligands in rheumatoid arthritis. Arthritis research & therapy. 2011;13(5):244.

40. Scott DL, Delamere JP, Walton KW. The distribution of fibronectin in the pannus in rheumatoid arthritis. Br J Exp Pathol 1981;62(4):362-8.
41. Wang Y, Khan A, Antonopoulos A, Bouché L, Buckley CD, Filer A, et al. Loss of α2-6 sialylation promotes the transformation of synovial fibroblasts into a pro-inflammatory phenotype in arthritis. Nature communications. 2021;12(1):2343.
42. Bindea G, Mlecnik B, Hackl H, Charoentong P, Tosolini M, Kirilovsky A, et al. ClueGO: a Cytoscape plug-in to decipher functionally grouped gene ontology and pathway annotation networks. Bioinformatics. 2009;25(8):1091-3.
43. Wang Y, Çil Ç, Harnett MM, Pineda MA. Cytohesin-2/ARNO: A Novel Bridge Between Cell Migration and Immunoregulation in Synovial Fibroblasts. Frontiers in immunology. 2021;12:809896.
44. Wang Y, Pan P, Khan A, Çil Ç, Pineda MA. Synovial Fibroblast Sialylation Regulates Cell Migration and Activation of Inflammatory Pathways in Arthritogenesis. Frontiers in immunology. 2022;13:847581.
45. Shekhani MT, Forde TS, Adilbayeva A, Ramez M, Myngbay A, Bexeitov Y, et al. Collagen triple helix repeat containing 1 is a new promigratory marker of arthritic pannus. Arthritis research & therapy. 2016;18:171.
46. Kilian KA, Bugarija B, Lahn BT, Mrksich M. Geometric cues for directing the differentiation of mesenchymal stem cells. Proceedings of the National Academy of Sciences of the United States of America. 2010;107(11):4872-7.
47. Knight E, Murray B, Carnachan R, Przyborski S. Alvetex®: polystyrene scaffold technology for routine three dimensional cell culture. Methods in molecular biology (Clifton, NJ). 2011;695:323-40.
48. Costello L, Darling N, Freer M, Bradbury S, Mobbs C, Przyborski S. Use of Porous Polystyrene Scaffolds to Bioengineer Human Epithelial Tissues In Vitro. Methods in molecular biology (Clifton, NJ). 2021;2273:279-96.
49. Hughes CS, Postovit LM, Lajoie GA. Matrigel: a complex protein mixture required for optimal growth of cell culture. Proteomics. 2010;10(9):1886-90.
50. Ahmad N, Colak B, Zhang D-W, Gibbs MJ, Watkinson M, Becer CR, et al. Peptide Cross-Linked Poly (Ethylene Glycol) Hydrogel Films as Biosensor Coatings for the Detection of Collagenase. Sensors (Basel, Switzerland). 2019;19(7).
51. Zhou Y, Zhou B, Pache L, Chang M, Khodabakhshi AH, Tanaseichuk O, et al. Metascape provides a biologist-oriented resource for the analysis of systems-level datasets. Nat Commun. 2019;10(1):1523.

52. Firestein MR, Abellar R, Myers MM, Welch MG. Increased trophoblast inclusions in placentas from prematurely born infants: A potential marker of risk for preterm neurodevelopmental outcomes. Placenta. 2017;60:61-3.
53. Smolen JS, Aletaha D, Barton A, Burmester GR, Emery P, Firestein GS, et al. Rheumatoid arthritis. Nat Rev Dis Primers. 2018;4:18001.
54. Karouzakis E, Rengel Y, Jungel A, Kolling C, Gay RE, Michel BA, et al. DNA methylation regulates the expression of CXCL12 in rheumatoid arthritis synovial fibroblasts. Genes Immun. 2011;12(8):643-52.
55. Ai R, Whitaker JW, Boyle DL, Tak PP, Gerlag DM, Wang W, et al. DNA Methylome Signature in Synoviocytes From Patients With Early Rheumatoid Arthritis Compared to Synoviocytes From Patients With Longstanding Rheumatoid Arthritis. Arthritis Rheumatol. 2015;67(7):1978-80.
56. Nakano K, Whitaker JW, Boyle DL, Wang W, Firestein GS. DNA methylome signature in rheumatoid arthritis. Ann Rheum Dis. 2013;72(1):110-7.
57. Nakano K, Boyle DL, Firestein GS. Regulation of DNA methylation in rheumatoid arthritis synoviocytes. J Immunol. 2013;190(3):1297-303.
58. Ai R, Hammaker D, Boyle DL, Morgan R, Walsh AM, Fan S, et al. Joint-specific DNA methylation and transcriptome signatures in rheumatoid arthritis identify distinct pathogenic processes. Nat Commun. 2016;7:11849.
59. Peck Y, Leom LT, Low PFP, Wang DA. Establishment of an in vitro three-dimensional model for cartilage damage in rheumatoid arthritis. J Tissue Eng Regen Med. 2018;12(1):e237-e49.
60. Aungier SR, Cartwright AJ, Schwenzer A, Marshall JL, Dyson MR, Slavny P, et al. Targeting early changes in the synovial microenvironment: a new class of immunomodulatory therapy? Ann Rheum Dis. 2019;78(2):186-91.
61. Gonzalez-Garcia C, Cantini M, Ballester-Beltran J, Altankov G, Salmeron-Sanchez M. The strength of the protein-material interaction determines cell fate. Acta Biomater. 2018;77:74-84.
62. Keselowsky BG, Collard DM, García AJ. Surface chemistry modulates fibronectin conformation and directs integrin binding and specificity to control cell adhesion. Journal of biomedical materials research Part A. 2003;66(2):247-59.
63. Llopis-Hernandez V, Cantini M, Gonzalez-Garcia C, Cheng ZA, Yang J, Tsimbouri PM, et al. Material-driven fibronectin assembly for high-efficiency presentation of growth factors. Sci Adv. 2016;2(8):e1600188.

64. Chandel K, Prakash M, Sinha A, Sharma A, Chouhan DK, Sandhu MS. Role of Shear Wave Elastography of Synovium to Differentiate Rheumatoid and Tubercular Arthritis. J Med Ultrasound. 2022;30(1):30-5.
65. Kucukural A, Yukselen O, Ozata DM, Moore MJ, Garber M. DEBrowser: interactive differential expression analysis and visualization tool for count data. 2019:1-12.
66. Shannon P, Markiel A, Ozier O, Baliga NS, Wang JT, Ramage D, et al. Cytoscape: a software environment for integrated models of biomolecular interaction networks. Genome Res. 2003;13(11):2498-504.

Funding.
Versus Arthritis Career Development Fellowship Award grant 21221 (MAP)
The Carnegie Trust for the Universities of Scotland Seed Award (MAP)
EPSRC PhD Studentship (MMH, MAP, MS)

Conflict of interests. Authors declare that they have no competing interests.

Data and materials availability: All data created or used during this study will be openly available from public repositories. Transcriptomic data, including raw sequencing data and processed read counts for each sample will be deposited in NCBI's Gene Expression Omnibus.

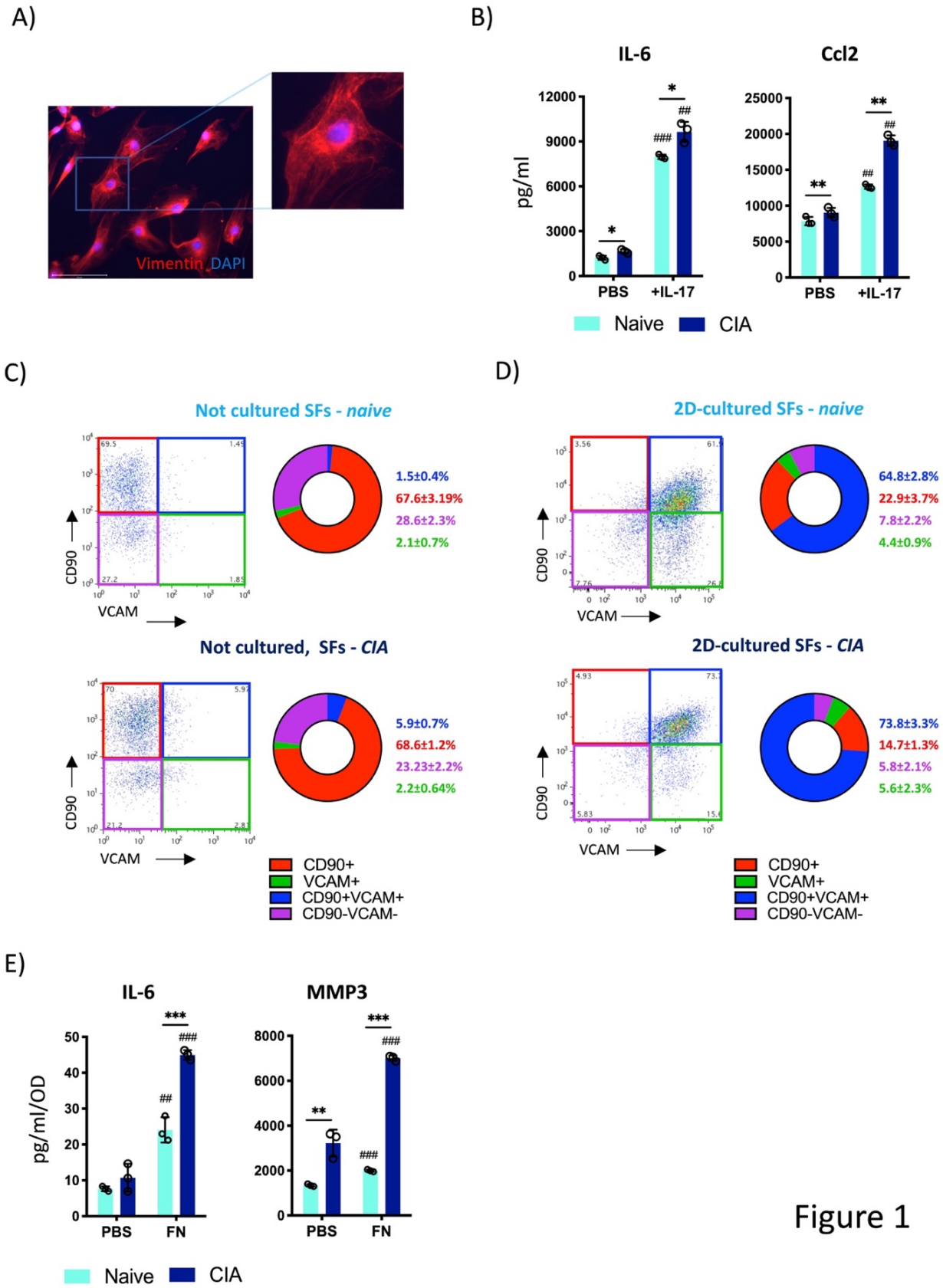
A)
Vimentin, DAPI
B)
IL-6
Ccl2
pg/ml
PBS
+IL-17
Naive
CIA
C)
Not cultured SFs - naive
1.5±0.4%
67.6±3.19%
28.6±2.3%
2.1±0.7%
Not cultured, SFs - CIA
5.9±0.7%
68.6±1.2%
23.23±2.2%
2.2±0.64%
CD90
VCAM
CD90+
VCAM+
CD90+VCAM+
CD90-VCAM-
D)
2D-cultured SFs - naive
64.8±2.8%
22.9±3.7%
7.8±2.2%
4.4±0.9%
2D-cultured SFs - CIA
73.8±3.3%
14.7±1.3%
5.8±2.1%
5.6±2.3%
E)
IL-6
MMP3
pg/ml/OD
PBS
FN
Naive
CIA

Figure 1

Figure 1. 2D cultured SFs show a non-physiological phenotype reactive to fibronectin-dependent immunomodulation. A) 2D cultured SFs cells were stained with anti-vimentin antibody (red) to visualize vimentin filaments by immunofluorescence. DAPI (blue) was used for counterstaining of nuclei. Scale bar: 100 μm. **B)** SFs were isolated from synovium of healthy or Collagen-Induced Arthritis (CIA) mice and expanded ex vivo until passages 3-4. SFs were then stimulated with recombinant IL-17 [10 ng/ml, 12h] or PBS as control. IL-6 and Ccl2 was measured in culture supernatants by ELISA. Data (pg/ml) are presented as mean ± SD, n=3 independent experiments. One-tail unpaired t-test was used for statistics, *$p < 0.05$, **$p < 0.01$. ###$p<0.001$, ##$p < 0.01$ compared with non-stimulated controls. **C-D)** Mouse synovium from healthy and CIA mice was digested and the expression of CD90 and VCAM-1 was evaluated by flow cytometry in cells directly isolated from the tissue [not cultured] (C) or following expansion in 2D for 3-4 passages [2D-cultured] (D). For in vivo cells, SFs were gated as live CD45-CD31-Podoplanin+. Pie charts show the proportion of CD90+VCAM- (red), CD90-VCAM+ (green), CD90+VCAM+ (blue) and CD90-VCAM- (purple) SFs. Numbers show percentage of positive SFs ± SD from 3 biological replicates. **E)** Naïve and CIA SFs expanded in 2D were cultured in FN-coated and non-treated control wells for 7 days. IL-6 and MMP3 were measured in cultured supernatants by ELISA. Cells were stained with crystal violet, washed and dissolved in SDS to quantify the amount of crystal violet (absorption at 495 nm) as an indirect measure of cell number for data normalization. Data (pg cytokine/ml/OD_{495}) are presented as mean ± SD, n=3 independent experiments. One-tail unpaired t-test was used for statistics, **$p < 0.01$, ***$p < 0.001$. ##$p < 0.01$, ###$p < 0.001$ compared with PBS control wells.

Non-cultured synovial fibroblast - CIA vs Naive

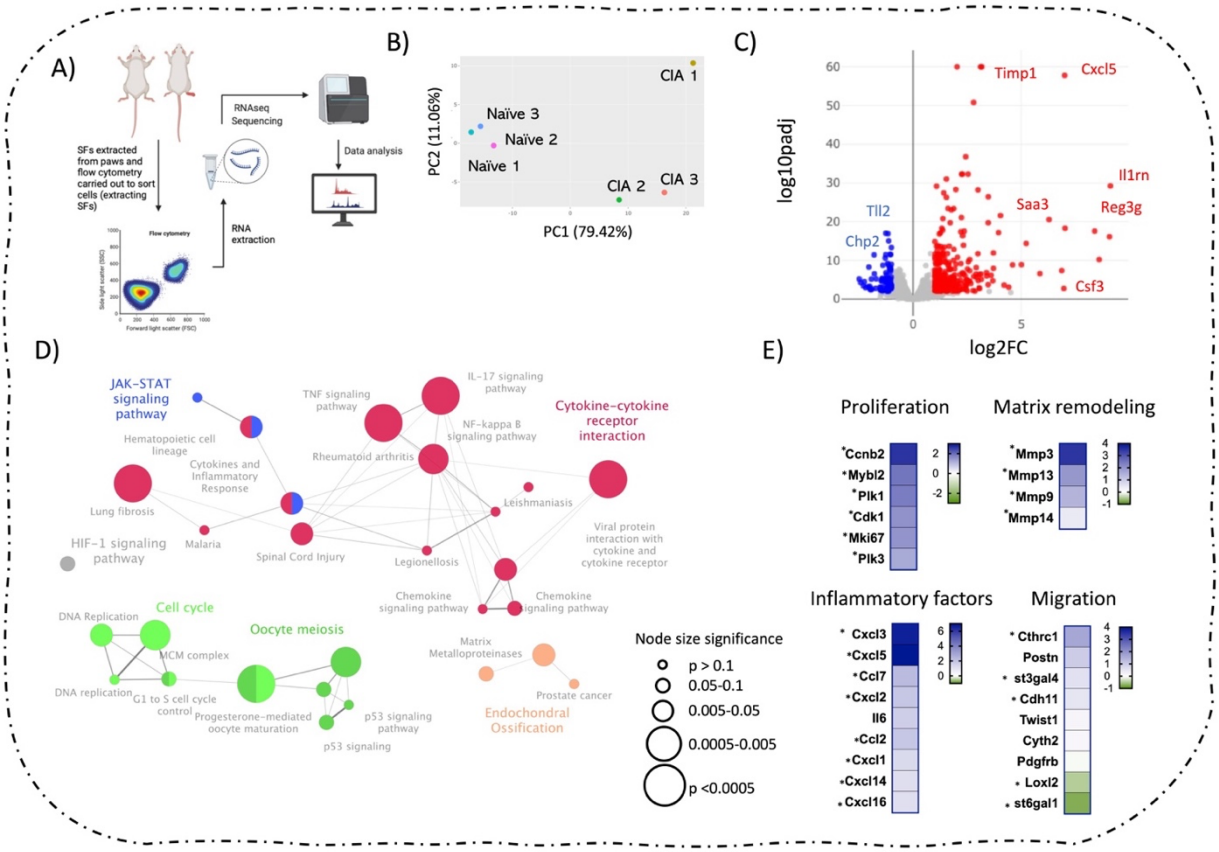

2D cultured synovial fibroblast – CIA vs Naive

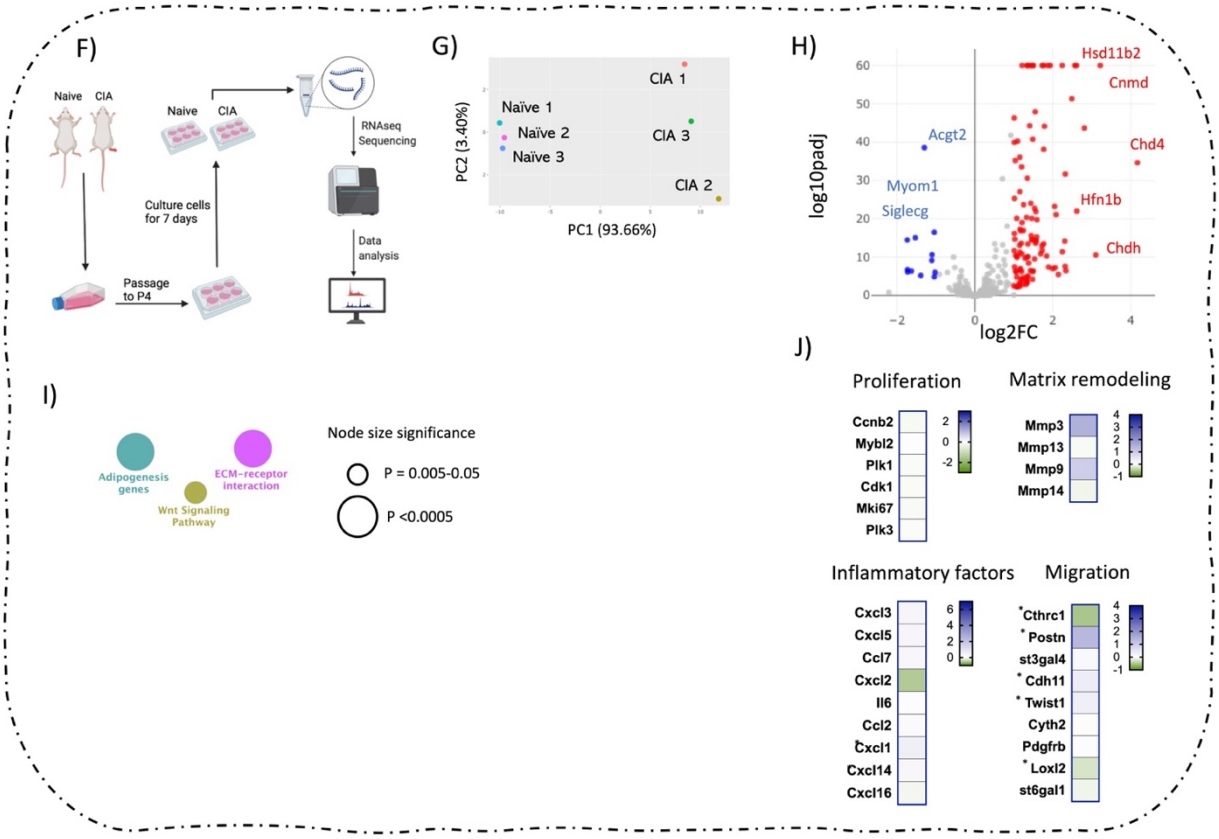

Figure 2

Figure 2. Transcriptomic phenotype of in vivo and 2D cultured arthritic SFs. **A,F)** Experimental strategy for bulk RNA-Seq studies of SFs in vivo **(A)** and expanded 2D **(F).** For in vivo studies (A-E, top panel), SFs were sorted by flow cytometry from healthy (n=3) and arthritic CIA mice (n=3). For 2D studies (F-J, bottom panel), synovial tissue was digested, and cells were cultured in 2D until passages 3-4. RNA was isolated and subjected to bulk RNA-Seq (75 bp paired-end, 30 M reads) to compare CIA versus naïve SFs transcriptomic profiles. **B-E)** Bioinformatic analysis of sorted naïve and CIA SFs of non-cultured cell: **B)** Principal component analysis. **C)** Differential expression (DE) of genes. **D**) Functional enrichment and network analysis from genes differentially up-regulated in arthritic cells. Terms are indicated as a node, and the size of the node indicates its significance as indicated. The most significantly expressed pathway in each network is shown in colored text. **E)** Supervised analysis of selected genes involved in cell proliferation, matrix remodeling, secretion of inflammatory mediators and migration. **G-J)** Bioinformatic analysis of 2D cultured naïve and CIA SFs: **G)** Principal component analysis. **H)** Differential expression (DE) of genes. **I**) Functional enrichment and network analysis. **J)** Supervised analysis of selected genes involved in cell proliferation, matrix remodeling, secretion of inflammatory mediators and migration. For C and H, all detected genes are plotted as a volcano plot where x = log2 Fold Change in CIA cells, y = log10 padj value. Genes that passed a threshold of padj < 0.01 and |log2foldChange| > 2 in DE analysis are colored in blue when they were downregulated and red when they were upregulated in SFs of arthritic (CIA) origin. Functional enrichment and network analysis in D and I was conducted by integration of KEGG, Wikipathways and CORUM datasets using the ClueGo plugin in cytoscape. Heatmaps in E and J represent the mean of log2Fold Change for each gene from the related bulk RNA-Seq analysis, n=3; * : DE genes, adjp < 0.01.

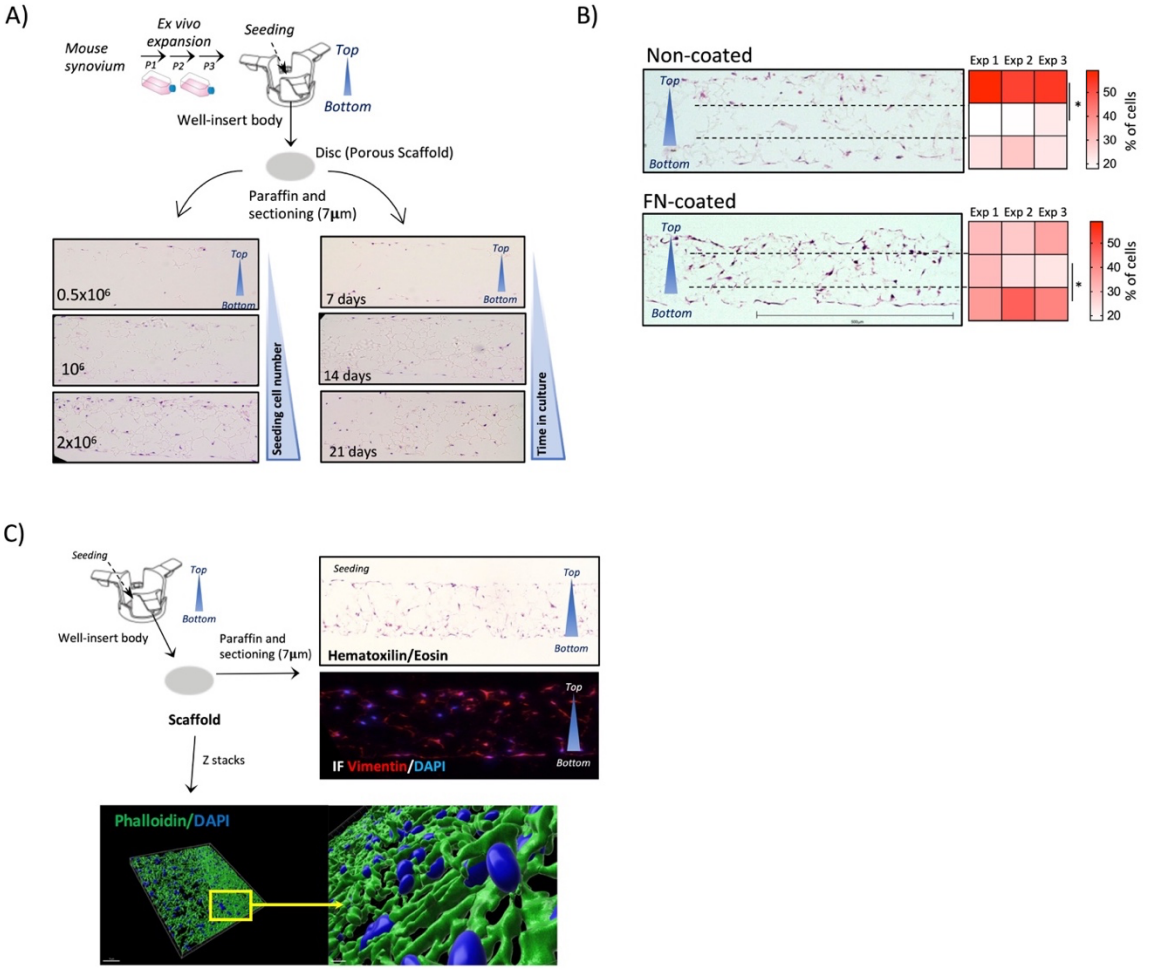
A)
Mouse synovium
Ex vivo expansion
P1
P2
P3
Seeding
Top
Bottom
Well-insert body
Disc (Porous Scaffold)
Paraffin and sectioning (7µm)
0.5x10⁶
10⁶
2x10⁶
Seeding cell number
7 days
14 days
21 days
Time in culture
B)
Non-coated
FN-coated
Exp 1 Exp 2 Exp 3
% of cells
C)
Well-insert body
Paraffin and sectioning (7µm)
Scaffold
Z stacks
Hematoxilin/Eosin
IF Vimentin/DAPI
Phalloidin/DAPI

Figure 3

Figure 3. Alvetex® scaffolds support 3D SF culture. A) Schematic representation of 3D Alvetex® scaffolds. Cells were expanded in 2D and then seeded on 3D fibronectin-coated scaffolds (seeding side indicated as 'top'). $0.5x10^6$, $1x10^6$ and $2x10^6$ SFs were initially seeded in 6-well inserts and then cultured for 14 weeks (left panels). $0.5x10^6$ SFs were seeded in 6-well inserts and cultured for 7, 14 and 21 days (right panels). Scaffolds were then fixated in formalin, and longitudinal sections (7 μm) were stained with hematoxilin and eoxin to evaluate cell number and distribution. **B)** Haemotoxylin and Eosin staining on naïve SFs cultured in non-coated scaffolds alone (PBS) or fibronectin (FN) coated. Images were taken on a EVOS brightfield microscope at x10 magnification (scale bar = 500 μm). Heatmaps show the percentage of cells in the indicated area of the scaffold (calculated with ImageJ software), as mean from technical triplicates from three independent experiments. Statistical significance was evaluated by two-way ANOVA, *$p<0.05$. **C)** Hematoxilin/eosin staining and immunofluorescence to detect vimentin (red) and DAPI (blue) was conducted in sections (7 μm) of FN-coated scaffolds containing naïve SFs ($1x10^6$ cells, 9 days in culture). Whole discs were fixed and stained with phalloidin (green) to visualise cytoskeleton organization and cell shape prior to acquisition of Z-stack images. DAPI (blue) was used as a counterstaining to visualise cell nuclei. Images were acquired using a Zeiss Confocal microscope (phalloidin/DAPI) staining and 3D reconstructions were done with Imaris software.

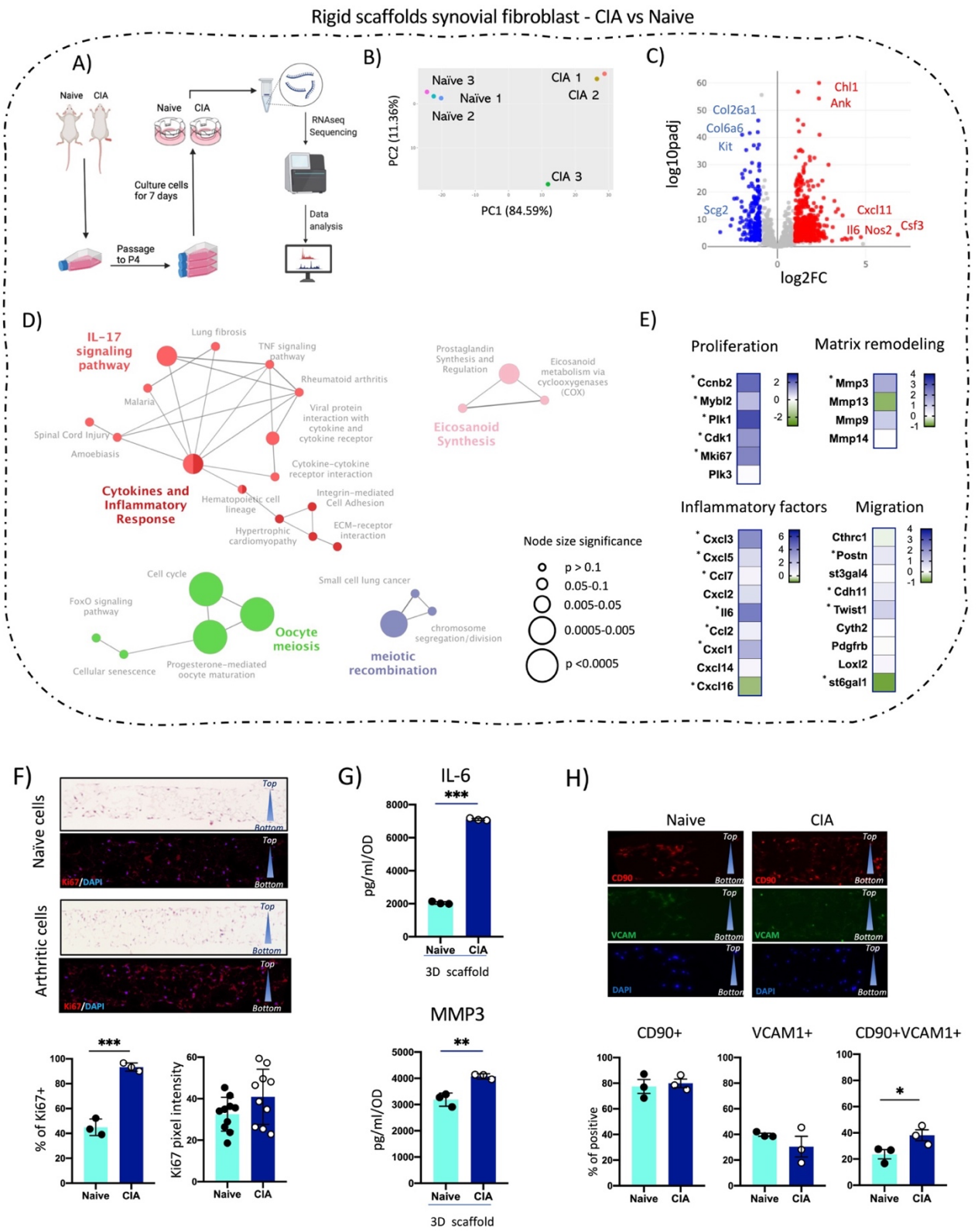
Rigid scaffolds synovial fibroblast - CIA vs Naive
A)
Naive
CIA
Culture cells for 7 days
RNAseq Sequencing
Data analysis
Passage to P4
B)
Naïve 3
Naïve 1
Naïve 2
CIA 1
CIA 2
CIA 3
PC2 (11.36%)
PC1 (84.59%)
C)
log10padj
log2FC
Col26a1
Col6a6
Kit
Scg2
Chl1
Ank
Cxcl11
Il6
Nos2
Csf3
D)
IL-17 signaling pathway
Lung fibrosis
TNF signaling pathway
Rheumatoid arthritis
Malaria
Viral protein interaction with cytokine and cytokine receptor
Spinal Cord Injury
Amoebiasis
Cytokine-cytokine receptor interaction
Cytokines and Inflammatory Response
Hematopoietic cell lineage
Integrin-mediated Cell Adhesion
Hypertrophic cardiomyopathy
ECM-receptor interaction
Prostaglandin Synthesis and Regulation
Eicosanoid metabolism via cyclooxygenases (COX)
Eicosanoid Synthesis
Cell cycle
FoxO signaling pathway
Oocyte meiosis
Cellular senescence
Progesterone-mediated oocyte maturation
Small cell lung cancer
chromosome segregation/division
meiotic recombination
Node size significance
p > 0.1
0.05-0.1
0.005-0.05
0.0005-0.005
p <0.0005
E)
Proliferation
Ccnb2
Mybl2
Plk1
Cdk1
Mki67
Plk3
Matrix remodeling
Mmp3
Mmp13
Mmp9
Mmp14
Inflammatory factors
Cxcl3
Cxcl5
Ccl7
Cxcl2
Il6
Ccl2
Cxcl1
Cxcl14
Cxcl16
Migration
Cthrc1
Postn
st3gal4
Cdh11
Twist1
Cyth2
Pdgfrb
Loxl2
st6gal1
F)
Naïve cells
Arthritic cells
Top
Bottom
Ki67/DAPI
% of Ki67+
Ki67 pixel intensity
Naive
CIA
G)
IL-6
pg/ml/OD
3D scaffold
MMP3
H)
Naive
CIA
CD90
VCAM
DAPI
CD90+
VCAM1+
CD90+VCAM1+
% of positive

Figure 4

Figure 4. Transcriptomic phenotype of arthritic SFs in 3D scaffolds. **A)** Experimental strategy, cells were expanded in 2D culture prior to culture in FN-coated scaffolds for 7 days. RNA was then isolated and subjected to bulk RNA-Seq (75 bp paired-end, 30 M reads) to compare CIA versus naïve SFs. **B-E)** Bioinformatic analysis. **B)** Principal component analysis, **C)** differential expression (DE) of genes, plotted as a volcano plot where x = log2 Fold Change in CIA cells, y = log10 padj value. Genes that passed a threshold of padj < 0.01 and |log2foldChange| > 2 in the arthritic (CIA) SFs are colored in blue [downregulated] and red [upregulated]. **D)** Functional enrichment and network analysis from genes differentially up-regulated in arthritic cells. Terms are indicated as a node, and the size of the node indicates its significance as indicated, colored text shows the most significant pathway for each network. Analysis was conducted by integration of KEGG, Wikipathways and CORUM datasets using the ClueGo plugin in Cytoscape. **E)** Supervised analysis of selected genes involved in cell proliferation, matrix remodeling, secretion of inflammatory mediators and migration. Heatmaps represent the mean of log2Fold Change from the bulk RNA-Seq analysis, n=3; * adjp < 0.01. **F)** Naïve and CIA SFs were cultured in FN-coated scaffolds for 7 days, sections were stained with hematoxilin/eosin and antibodies against Ki67 (red) and DAPI (blue) for immunofluorescence. Percentage of Ki67+ cells was calculated, dots represent mean of technical triplicates from independent experiments (n=3), error bars = SD, *** = p < 0.001 calculated by two-tailed unpaired t test. Pixel intensity for Ki67 staining was calculated using image J, each dot represents individual cells from one representative experiment. **G)** Naïve and CIA SFs were cultured in FN-coated scaffolds (7 days), medium was replaced and collected 24 hours later to measure IL-6 and MMP3 in supernatants by ELISA. Crystal violet was used (OD 495 nm) as an indirect measure of cell number for data normalization. Data (pg cytokine/ml/OD_{495}) are presented as mean ± SD, n=3 independent experiments. Two-tail unpaired t-test was used for statistics, **p < 0.01, ***p < 0.001. **H)** Sections containing naïve and CIA SFs were stained with against CD90 and VCAM-1 for immunofluorescence analysis. Percentage of CD90+, VCAM+ and CD90+VCAM-1+ was calculated using ImageJ, each dot shows mean of pixel intensity from one independent experiment (n=3), * = p<0.05 calculated by one-tailed unpaired t test.

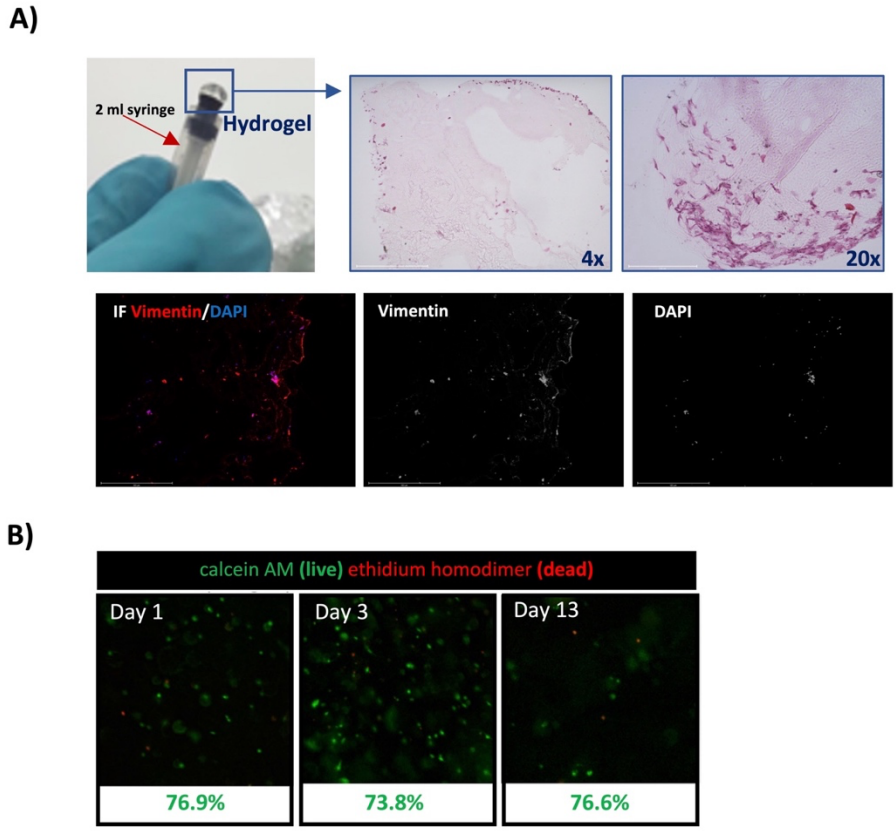

Figure 5

Figure 5: SFs distribution and cell viability in 3D FNPEG hydrogels. A) Photographic image of FNPEG hydrogel. Sections of non-degradable hydrogels containing naive SFs (7 days of culture) were prepared and stained with hematoxilin and eosin (histochemistry) or anti-vimentin antibodies and DAPI (immunofluorescence, red and blue respectively). **B)** Cellular viability of naïve SFs cultured in non-degradable FNPEG hydrogels. Representative images of SFs in FNPEG gels stained with calcein AM (live, green) and ethidium homodimer (dead, red) viability staining kit at days 1, 3 and 7.

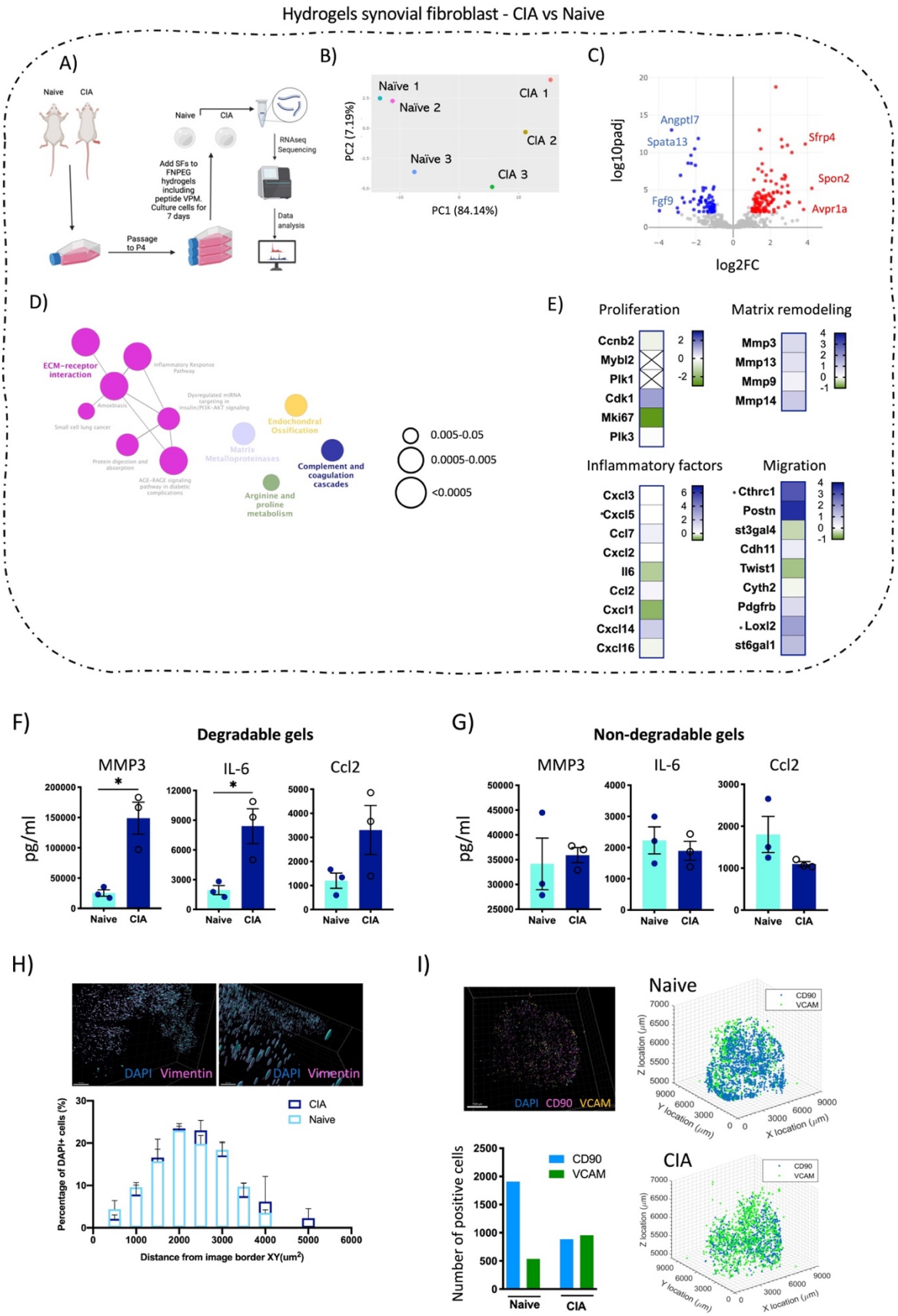
Hydrogels synovial fibroblast - CIA vs Naive
A)
Naive
CIA
Add SFs to FNPEG hydrogels including peptide VPM. Culture cells for 7 days
RNAseq Sequencing
Data analysis
Passage to P4
B)
Naïve 1
Naïve 2
Naïve 3
CIA 1
CIA 2
CIA 3
PC2 (7.19%)
PC1 (84.14%)
C)
Angptl7
Spata13
Fgf9
Sfrp4
Spon2
Avpr1a
log10padj
log2FC
D)
ECM-receptor interaction
Inflammatory Response Pathway
Amoebiasis
Small cell lung cancer
Protein digestion and absorption
Endochondral Ossification
Matrix Metalloproteinases
Complement and coagulation cascades
Arginine and proline metabolism
0.005-0.05
0.0005-0.005
<0.0005
E)
Proliferation
Ccnb2
Mybl2
Plk1
Cdk1
Mki67
Plk3
Matrix remodeling
Mmp3
Mmp13
Mmp9
Mmp14
Inflammatory factors
Cxcl3
Cxcl5
Ccl7
Cxcl2
Il6
Ccl2
Cxcl1
Cxcl14
Cxcl16
Migration
Cthrc1
Postn
st3gal4
Cdh11
Twist1
Cyth2
Pdgfrb
Loxl2
st6gal1
F)
Degradable gels
MMP3
IL-6
Ccl2
pg/ml
Naive
CIA
G)
Non-degradable gels
MMP3
IL-6
Ccl2
pg/ml
Naive
CIA
H)
DAPI Vimentin
DAPI Vimentin
CIA
Naive
Percentage of DAPI+ cells (%)
Distance from image border XY(um²)
I)
DAPI CD90 VCAM
Naive
CD90
VCAM
Z location (μm)
Y location (μm)
X location (μm)
CIA
Number of positive cells
CD90
VCAM
Naive
CIA

Figure 6

Figure 6. Transcriptomic phenotype of arthritic SFs in 3D FNPEG hydrogels. **A)** Experimental strategy, cells were expanded in 2D culture prior to culture in FNPEG degradable hydrogels for 3 days. RNA was then isolated and subjected to bulk RNA-Seq (75 bp paired-end, 30 M reads) to compare CIA versus naïve SFs. **B-E)** Bioinformatic analysis. **B)** Principal component analysis, **C)** differential expression (DE) of genes, plotted as a volcano plot where x = log2 Fold Change in CIA cells, y = log10 padj value. Genes that passed a threshold of padj < 0.01 and |log2foldChange| > 2 in the arthritic (CIA) SFs are colored in blue [downregulated] and red [upregulated]. **D)** Functional enrichment and network analysis from genes differentially up-regulated in arthritic cells. Terms are indicated as a node, and the size of the node indicates its significance as indicated, colored text shows the most significant pathway for each network. Analysis was conducted by integration of KEGG, Wikipathways and CORUM datasets using the ClueGo plugin in Cytoscape. **E)** Supervised analysis of selected genes involved in cell proliferation, matrix remodeling, secretion of inflammatory mediators and migration. Heatmaps represent the mean of log2Fold Change from the bulk RNA-Seq analysis, n=3; * padj < 0.01. **F-G)** MMP3, IL-6 and Ccl2 was quantified by ELISA in the supernatants of Naïve and CIA SFs cultured in degradable (F) and non-degradable (G) hydrogels. Each dot represents the mean of independent experiments (n=3), analyzed in technical triplicates. Error bars = SD, **p < 0.01, ***p < 0.001 by two-tail unpaired t-test. **H)** Non-degradable FNPEG hydrogels were stained with anti-vimentin antibodies (red) and DAPI (blue). Images were taken using a widefield microscope in z steps of ~10 μm tile scanned, merged and deconvoluted. Whole scanned hydrogels were analyzed with Imaris software to quantify the distance of each cell (located by DAPI staining) to the image border. Percentage of cells as indicated distance is shown in the histogram for naïve and CIA SFs. Data show mean of 4 independent experiments, error bars = SD. I) Non-degradable FNPEG hydrogels were stained with anti-CD90 and anti-VCAM-1 antibodies, and number of positive cells were calculated with Imaris software. Data are from one experiment, corresponding 3D scatter plots were created in Matlab using X,Y,Z positions of CD90+ and VCAM+ cells.

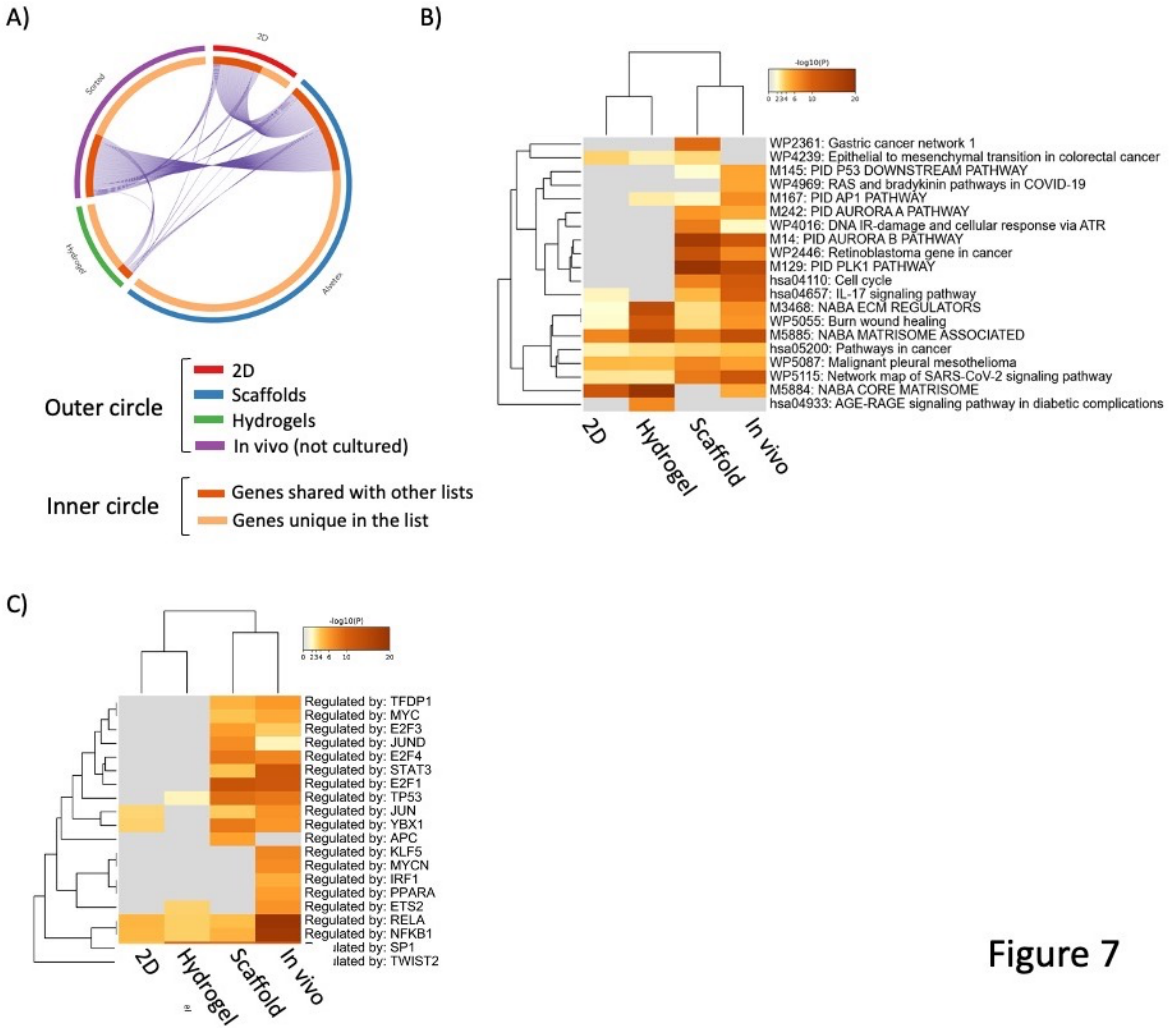

Figure 7. Comparative meta-analysis across in vivo, 2D and 3D cultured arthritic SFs RNA-Seq datasets. Differentially expressed genes in CIA SFs compared to healthy controls in not cultured cells and cells cultured in 2D, 3D rigid scaffolds and FNPEG hydrogels were compared using the bioinformatic tool Metascape. **A)** Circos plot representing significantly up-regulated genes overlapping in not cultured cells, 2D cultured cells and cells in 3D rigid scaffolds and FNPEG hydrogels. (Groups represented on the arc outside; red: 2D, blue: Alvetex® scaffold, green: FNPEG hydrogels). **B)** Enriched ontology clusters in CIA SFs compared to healthy cells in all systems tested. Clusters were hierarchically clustered into a tree based on Kappa-statistical similarities among their gene memberships. **C)** TRRUST (Transcriptional Regulatory Relationships Unraveled by Sentence-based Text mining, https://www.grnpedia.org/trrust/) was used to identify activation of Transcription Factor-specific pathways in CIA SFs based on literature curation. The heatmap cells are colored by their p-values, white cells indicate the lack of enrichment for that term in the corresponding gene list. All results were generated with the bioinformatic tool Metascape.

A)

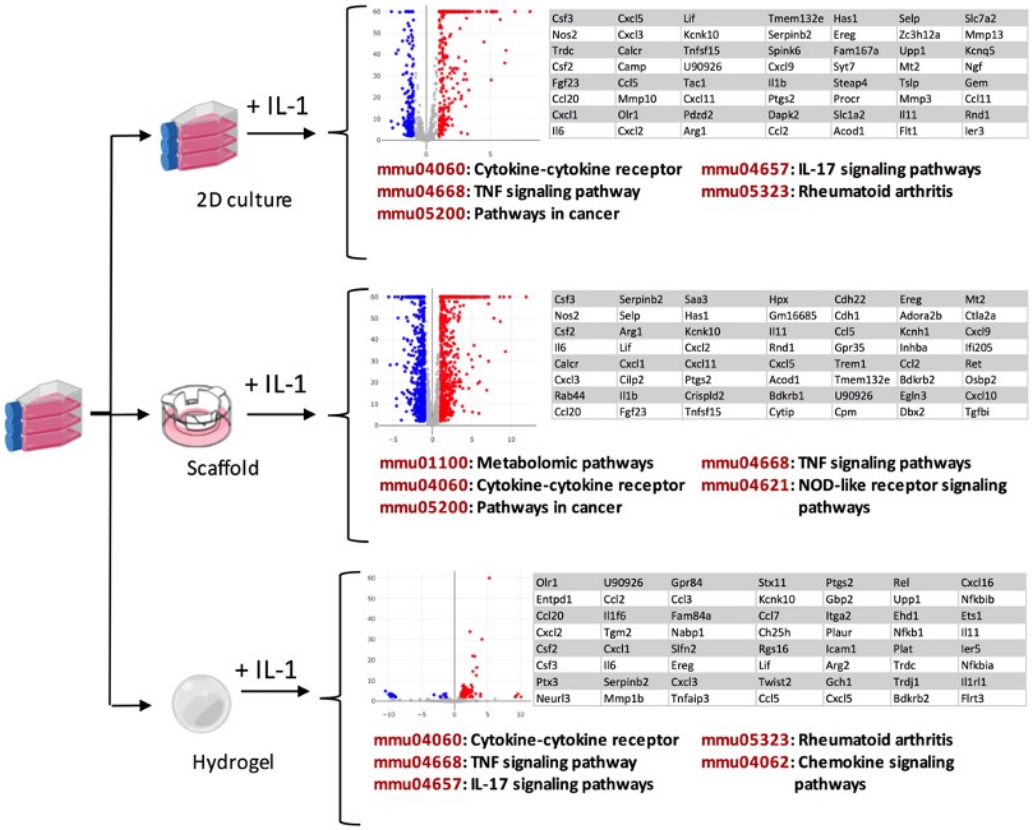

Csf3	Cxcl5	Lif	Tmem132e	Has1	Selp	Slc7a2
Nos2	Cxcl3	Kcnk10	Serpinb2	Ereg	Zc3h12a	Mmp13
Trdc	Calcr	Tnfsf15	Spink6	Fam167a	Upp1	Kcnq5
Csf2	Camp	U90926	Cxcl9	Syt7	Mt2	Ngf
Fgf23	Ccl5	Tac1	Il1b	Steap4	Tslp	Gem
Ccl20	Mmp10	Cxcl11	Ptgs2	Procr	Mmp3	Ccl11
Cxcl1	Olr1	Pdzd2	Dapk2	Slc1a2	Il11	Rnd1
Il6	Cxcl2	Arg1	Ccl2	Acod1	Flt1	Ier3

Csf3	Serpinb2	Saa3	Hpx	Cdh22	Ereg	Mt2
Nos2	Selp	Has1	Gm16685	Cdh1	Adora2b	Ctla2a
Csf2	Arg1	Kcnk10	Il11	Ccl5	Kcnh1	Cxcl9
Il6	Lif	Cxcl2	Rnd1	Gpr35	Inhba	Ifi205
Calcr	Cxcl1	Cxcl11	Cxcl5	Trem1	Ccl2	Ret
Cxcl3	Cilp2	Ptgs2	Acod1	Tmem132e	Bdkrb2	Osbp2
Rab44	Il1b	Crispld2	Bdkrb1	U90926	Egln3	Cxcl10
Ccl20	Fgf23	Tnfsf15	Cytip	Cpm	Dbx2	Tgfbi

Olr1	U90926	Gpr84	Stx11	Ptgs2	Rel	Cxcl16
Entpd1	Ccl2	Ccl3	Kcnk10	Gbp2	Upp1	Nfkbib
Ccl20	Il1f6	Fam84a	Ccl7	Itga2	Ehd1	Ets1
Cxcl2	Tgm2	Nabp1	Ch25h	Plaur	Nfkb1	Il11
Csf2	Cxcl1	Slfn2	Rgs16	Icam1	Plat	Ier5
Csf3	Il6	Ereg	Lif	Arg2	Trdc	Nfkbia
Ptx3	Serpinb2	Cxcl3	Twist2	Gch1	Trdj1	Il1rl1
Neurl3	Mmp1b	Tnfaip3	Ccl5	Cxcl5	Bdkrb2	Flrt3

B)

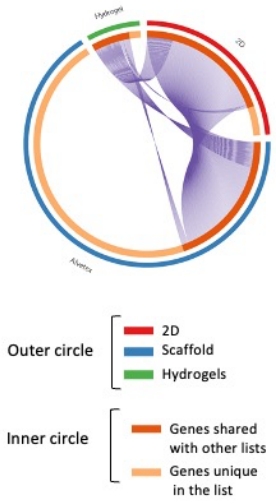

C)

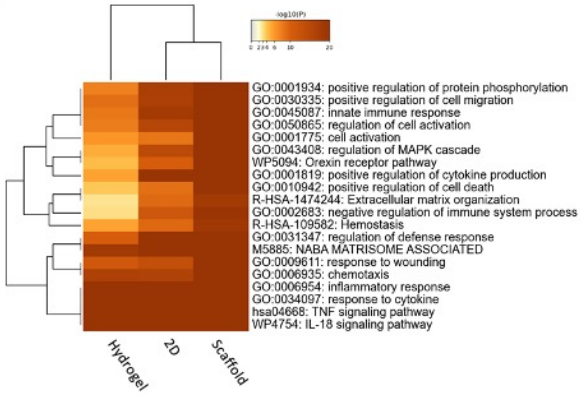

D)

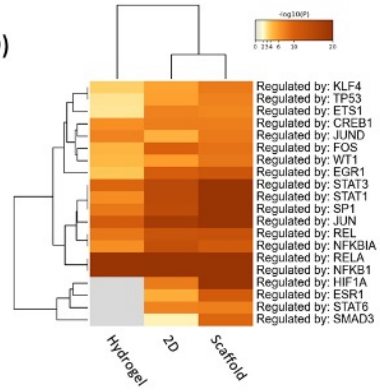

Figure 8

Figure 8. SFs responses to IL-1β stimulation in 2D and 3D systems. SFs cultured in 2D conditions, and cells subsequentially transferred to Alvetex® scaffolds and FNPEG hygrogels were stimulated with IL-1β (10 ng/ml, 6 hours), when RNA was extracted to conduct RNA-Seq experiments (n=3, 75 bp paired-end, 30 M reads). **A)** Differential expression (DE) of genes, plotted as a volcano plot where x = log2 Fold Change in CIA cells, y = log10 padj value. Genes that passed a threshold of padj < 0.01 and |log2foldChange| > 2 in the arthritic (CIA) SFs are colored in blue [downregulated] and red [upregulated]. Tables show the top-50 up-regulated genes in response to IL-1β for each condition. Significantly enriched KEGG pathways are shown. **B)** Circos plot show how IL-1β upregulated genes overlap in 2D and 3D systems (On the arc outside, red: 2D, blue: Alvetex® scaffold, green: FNPEG hydrogels). On the arc inside, each gene is assigned a spot in the arc, dark orange = genes shared in multiple lists, light orange = gene unique to that list. Purple lines link the same gene that are shared by multiple gene lists. **C)** Enriched ontology clusters in 2D and 3D systems upon IL-1β stimulation were identified and hierarchically clustered into a tree based on Kappa-statistical similarities among their gene memberships. **D)** DE expressed genes upon IL1β were applied to TRRUST (Transcriptional Regulatory Relationships Unraveled by Sentence-based Text mining, https://www.grnpedia.org/trrust/) analysis to identify activation of Transcription Factor-specific pathways based on literature curation. In heatmaps, cells are colored by their p-values, white cells indicate the lack of enrichment for that term in the corresponding gene list. All results were generated with the bioinformatic tool Metascape.